Atomic scale models of dislocation cores in minerals: progress and prospects

Andrew M. Walker[1,*], Philippe Carrez[2] and Patrick Cordier[2]

[1] Department of Earth Sciences, University College London, Gower Street, London, WC1E 6BT, UK

[2] Unité Matériaux et Transformations, UMR 8207 CNRS-Université Lille 1, Univ Lille Nord de France, F-59655 Villeneuve d'Ascq, France

*E-mail: a.walker@ucl.ac.uk

Abstract

Recent advances in computer simulation at the atomic scale have made it possible to use these methods to study the structure and behaviour of the cores of dislocations in minerals. Such simulation offers the possibility of understanding and predicting the dislocation-mediated properties of minerals such as mechanisms of plastic deformation, pipe diffusion and crystal growth. In this review the three major methods available for the simulation of dislocation cores are described and compared. The methods are: (i) Cluster based models which combine continuum elastic theory of the extended crystal with an atomistic model of the core. (ii) Dipole models which seek to cancel the long range elastic displacement caused by the dislocation by arranging for the simulation to contain several dislocations with zero net Burgers vector, thus allowing a fully periodic super-cell calculation. (iii) The Peierls-Nabarro approach which attempts to recast the problem so that it can be solved using only continuum based methods, but parameterizes the model using results from atomic scale calculations. The strengths of these methods are compared and illustrated by some of the recent studies of dislocations in mantle silicate minerals. Some of the outstanding unresolved problems in the field are discussed.

Keywords: computer modelling, dislocations, plasticity, core structure, deformation.

This is the author's pre-print (draft before refereeing) of a review article that appeared in the June 2010 issue of *Mineralogical Magazine*. The peer-reviewed, formatted, edited and published version can be found at http://dx.doi.org/10.1180/minmag.2010.074.3.381 and cited as: Walker, A.M., Carrez, P. and Cordier, P. (2010) "Atomic scale models of dislocation cores in minerals: progress and prospects" *Mineralogical Magazine*, 74:381-413.

Introduction

Many of the properties of minerals are controlled or influenced by the presence of dislocations, line defects in their crystal structure. Knowledge of the detailed structure of dislocation cores is essential to understand many processes in minerals. For example, the plastic deformation of minerals at high temperature is often controlled by the glide or climb of dislocations (Poirier, 1985), processes which are directly controlled by atomic scale changes in the dislocation core. During glide controlled plasticity, the dislocation mobility is permitted as the core structure changes to overcome the resistance imposed by the periodic crystal lattice, the Peierls potential. During climb controlled deformation, interactions between point defects and dislocations allow the dislocation to move out of the glide plane and around larger-scale obstacles. Mineral growth from solution, especially at low super-saturation, is enhanced by the emergence of screw dislocations at the crystal surface (Burton *et al*., 1949); a process that results in the formation of characteristic growth spirals in minerals as diverse as rock salt (Sunagawa and Tsukamoto, 1972), calcite (Davis *et al*., 2000) and some zeolites (Dumrul *et al*., 2002). The presence of line defects in crystals can also open pathways for the rapid diffusion of point defects, an effect that has been measured in simple materials such aluminium (Legros *et al*., 2008), MgO (Narayan and Washburn, 1972, Sakaguchi *et al*., 1992) and Y_2O_3 (Gaboriaud, 2009) and could perturb trace element geochemistry (Reddy *et al*., 2006). This pipe-diffusion mechanism modifies high temperature diffusion controlled deformation mechanisms, complicating the relationship between point defect diffusion and deformation (Frost and Ashby, 1982). Dislocations also play a role in the formation of sub-grains during deformation. Indeed, a low angle sub-grain boundary is a particular alignment of dislocations that can form during deformation in order to minimise the long range stress field.

Although dislocations can be imaged routinely using electron microscopy (see Cordier, 2002, for a recent review) it has only become possible to infer anything about the structure of the dislocation core from experiment recently, and in a few special cases. One example is a study of a [100](010) edge dislocation from a low-angle grain boundary in forsterite (Johnson *et al*., 2004). This study made use of a combination of high resolution transmission electron microscopy (HRTEM) and geometric phase analysis (Hÿtch *et al*., 1998; 2003) to map the deformation of the crystal structure around the dislocation, resolving displacements of less than 0.1 Å. This is sufficient to reveal the non-linear displacement field around the dislocation core but the approach does not directly constrain the core structure. Work that does experimentally constrain the structure of dislocation cores makes use of HRTEM, as illustrated by the study of a [001](110) dislocation in $SrTiO_3$ perovskite (Jia *et al*., 2005). This work is possible thanks to the recent developments in aberration (Cs) corrections in TEM. It shows in this case that the dislocation core is extended and nonstoichiometric. Despite these advances, the determination of the structure of dislocation cores in

minerals remains extremely challenging. However, knowledge of the structure of the core is important to fully understand dislocation mediated processes in minerals. In order to circumvent the formidable experimental challenges it is necessary to turn to atomic scale simulation of dislocation cores. Such simulations have been performed for structurally simple materials including metals and rock salt structured crystals for many years but until recently there were no computational studies of dislocation cores in silicate minerals. During the last five years this situation has changed and much progress has been made in developing methods suitable for the modelling of dislocation cores in minerals. These methods have been used to provide the atomic scale structure of dislocation cores in order to explain experimental observations, and to probe dislocation behaviour under extreme conditions in order to predict deformation behaviour at pressures beyond those accessible to experiment. This article reviews the recent progress in atomic scale simulation methods to model the cores of dislocations in minerals, outlines the major advances made by applying these methods, and describes some of the remaining problems still to be tackled.

Although atomic scale modelling of dislocations in minerals is a relatively recent advance, computational simulation methods have been used to overcome experimental limitations and study the atomic-scale detail of the cores dislocations in crystalline solids for over four decades and the basic theory of dislocations has been established since early in the 19th Century. We don't seek to review the whole subject but instead concentrate on the methods as they are applied to minerals. However, significant overlap between this work and previous review articles is inevitable. General introductions to dislocation theory many books and a multitude of review articles (e.g. Christian and Vítek, 1970). A gentle introduction to the theory can be found in Hull and Bacon (1984) while a comprehensive survey has been made by Hirth and Lothe (1984). Reviews of techniques for the atomic scale simulation of dislocation cores are largely restricted to the consideration of metals and structurally simple semiconductors (e.g. Schoeck, 2005; Woodward, 2005) or multi-scale modelling of deformation (Cordier *et al*., 2005). The review is split broadly into three parts. First, the three major approaches to modelling dislocations: cluster based embedded models, fully periodic dipole models and the semi-continuum Peierls-Nabarro model, are described. Second, the applications of these models to mantle minerals are reviewed. Third, some of the new directions and remaining difficulties are discussed. Before this we recall some of the major features of dislocations and discuss some of their important properties.

Background

The study of dislocations has two historical origins. The original concept of the dislocation, the singularity formed by the deformation of a multiply connected elastic continuum, was systematically developed by Volterra (1907) and named by Love (1920). Conceptually a Volterra

dislocation is introduced into an elastic body by introducing a cut from the edge to the centre of the body, translating the two sides of the cut relative to each other such that the sides remain parallel, then cementing the cut surfaces together before allowing the body to relax to elastic equilibrium (Figure 1). The equivalent procedure where the sides are rotated instead of translated leads to the formation of a disinclination, but these are not generally found in minerals. In order to describe the formation of a dislocation using using continuum theory it is first necessary to remove a small amount of material from the centre of the elastic body, where the cut will terminate, and depending on the direction of relative movement across the cut it may be necessary to add or remove material. The equations giving the displacements and energy stored by the dislocation in an elastically isotropic body are well known (e.g. Hull and Bacon, 1984). In the case where the displacement is of magnitude b and is in a direction parallel to the terminating line at the end of the cut (a screw dislocation, defined more formally below) the displacement field is given by:

$$\begin{aligned} u_x &= 0 \quad , \\ u_y &= 0 \quad , \\ u_z &= \frac{b}{2\pi} \arctan \frac{y}{x} \quad , \end{aligned} \tag{1}$$

where the notation used in this and other equations are given in Table 1. Equation 1 shows that any point in the elastic body (x,y) simply moves parallel to the dislocation line, such that a 360° rotation about the line corresponds to a displacement equal to the displacement applied across the cut, which can no longer be distinguished. In the case shown in Figure 1, where the displacement is perpendicular to the edge of the cut surface (an edge dislocation), the solution is slightly more complex. For an isotropic body with displacement along the x axis, the displacement of any point is given by:

$$\begin{aligned} u_x &= \frac{b}{2\pi} \left[\arctan\left(\frac{y}{x}\right) + \frac{xy}{2(1-\nu)\,(x^2+y^2)} \right] \quad , \\ u_y &= -\frac{b}{2\pi} \left[\frac{1-2\nu}{4(1-\nu)} \ln\left(x^2+y^2\right) + \frac{x^2-y^2}{4(1-\nu)\,(x^2+y^2)} \right] \quad , \\ u_z &= 0 \quad . \end{aligned} \tag{2}$$

One important feature of Equations 1 and 2 is that the deformation field does not change between locations along lines parallel to the dislocation line; for any given value of x and y the three components of the displacement field are equal for all values of z. This symmetry is a general feature of all straight dislocations and is used extensively in dislocation modelling. The stored energy in the elastic body increases as a result of introducing the dislocation. When introduced into a body of radius r (with a central hole radius r_0) the additional energy is given by:

$$E = \frac{Kb^2}{4\pi} \ln\left(\frac{r}{r_0}\right) \qquad (3)$$

For a screw dislocation the constant K is the shear modulus, μ, while for an edge dislocation it is given by $\mu/(1-\nu)$, where ν is Poisson's ratio.

The second origin of the study of dislocations came from the realisation that the theoretical strength of a perfect crystal is orders of magnitude higher then the strength found when experimentally deforming real crystals. This led the idea that dislocation-like defects may provide an explanation (Prandtl, 1928; Dehlinger, 1929) and the description of edge dislocations in crystals (Taylor, 1934; Orowan, 1934; Polanyi, 1934). Screw and mixed dislocations were first introduced by Burgers (1939) in a paper that is often regarded to have begun the systematic development of the theory of dislocations in crystals. The general geometry of an edge dislocation in a simple crystal, and the terms used to describe it, are shown in Figure 2. It is first necessary to distinguish regions of 'good' crystal, volumes where the atoms can be unambiguously mapped to equivalent atoms in a perfect reference crystal by allowing small displacements compared to the inter-atomic separation, from regions of 'bad' crystal, volumes where no such correspondence exists (Frank, 1951). Real crystals always contain some 'bad' crystal, for example near the core of dislocation lines and close to point defects, and linear elasticity theory cannot be applied to these regions. A closed circuit can be defined in the reference crystal and mapped onto atoms in the good part of a real crystal. If the circuit is threaded by a dislocation line (as in the case of circuit marked by the smaller arrows in Figure 2) then it is no longer closed in the real crystal and is known as a Burgers circuit. The vector measuring the failure of the closure is known as the Burgers vector (the large arrow in Figure 2, but see Bilby and Smith, 1956). The concept of the Burgers circuit can also be used to define the dislocation line (the z axis in Figure 2), as the locus around which Burgers circuits are not closed. When constructing a Burgers vector it is necessary to choose a convention for the direction of the Burgers vector (which could go from the start to the finish of the circuit or be reversed and can refer to a closed circuit in the real or reference crystal) and of the dislocation line (right handed or left handed). In Figure 2 the FS/RH convention (Bilby *et al*., 1955) is used, where the Burgers vector goes from the finish to the start of the closed right handed circuit in the reference crystal and the positive direction of the vector describing the dislocation line is out of the page towards the reader. For a straight dislocation line the character of the dislocation can be defined by the angle between a vector describing the dislocation line and the Burgers vector. If the two directions are orthogonal then the dislocation is an edge dislocation (shown in Figures 1 and 2), if they are parallel the dislocation is a screw dislocation, otherwise the dislocation has mixed character. For edge and mixed dislocations, the plane containing the dislocation line and the Burgers vector is know as the

glide plane (the *x*-*z* plane in Figure 2). The bad crystal around the dislocation line is known as the dislocation core and only the behaviour of the crystal away from the core can be treated using continuum elasticity.

There is a close relationship between the two descriptions of dislocations given above. Away from the dislocation line, in the region of good crystal, the deformation induced by the dislocation can be described by linear elasticity. This means that the elastic description of the dislocation is sufficient to describe the structure, stress, strain and excess energy of the extended crystal. However, there is one important constraint on the displacement across the cut surface and thus the Burgers vector allowed in a dislocation in a crystal. For the cut surface to be indistinguishable the crystal structure must be continuous across it. In turn this means that the displacement must result in the crystal structure 'matching up', resulting in the important result that the Burgers vector must be equal to a lattice vector. A second consideration is that the elastic description of the dislocation breaks down close to the dislocation line. In the description of dislocations in crystals the discrete atomic structure circumvents this, but results in a core structure that is hard to predict from the structure of the dislocation-free perfect crystal. In general the core will have a different energy to the same volume of perfect crystal, and Equation 3 is modified to account for this:

$$E = E_{(\text{core})} + \frac{Kb^2}{4\pi} \ln\left(\frac{r}{r_0}\right) \qquad (4)$$

where $E_{(\text{core})}$ is the energy stored in the dislocation core and r_0 is now the radius of the core. Because the structure of the core can be different to that of the strained perfect crystal, the core may occupy a different volume in the dislocation free and dislocated crystal. The core of the dislocation can thus apply forces on the extended crystal around the core which results in additional deformation, beyond that predicted from linear elasticity alone.

The major problem when simulating dislocations is due to the fact that all of the atoms in the crystal containing the dislocation are significantly displaced by its presence, atoms away from the core are not in the same locations as atoms in a perfect reference crystal. Indeed, the long-range displacement field is proportional to $1/r$. This means that the modelling approaches used to study point defects and surfaces, where the atomic structure away from the defect is identical to the structure of a perfect reference crystal, are not available. The various approaches to modelling dislocation cores described below side-step this issue in different ways. The cluster based methods combine continuum elastic theory of the extended crystal with an atomistic model of the core. Dipole models seek to cancel the long range elastic displacements by arranging for the simulation to contain several dislocations with zero net Burgers vector. The Peierls-Nabarro approach attempts to

recast the problem so that it can be solved using only continuum based methods, but parameterizes the model using results from atomic scale calculations.

Cluster models

The first class of approaches to the atomic scale modelling of dislocation cores is often described as the 'cluster' based approach. The idea is to take advantage of the symmetry of the Volterra dislocation to build a model using periodic boundary conditions along the dislocation line while only including a finite cluster of atoms perpendicular to the dislocation line. The resulting simulation cell is shown in Figure 3. This natural approach results in a model containing a single isolated dislocation, but care must be taken to avoid introducing spurious interactions between the edge of the simulated system and the dislocation core. The approach is similar in spirit to models of point defects and surfaces, where the defect is shielded from the surrounding vacuum by layers of atoms that represent perfect crystal, but instead of perfect crystal the dislocation is shielded by an elastically deformed crystal. This implies the need to couple an atomistic model of the dislocation core with elastic models of the extended crystal. These models can include very long range elastic effects and at this level the system can be considered to contain an isolated dislocation in an infinite crystal.

Coupling elastic and atomistic models

In coupling the core to the extended crystal there are four related issues that must be considered. First, it is necessary to be able to cope with the fact that minerals are generally not elastically isotropic so anisotropic elasticity must be used to describe the extended crystal. Second, the way that the elastic and atomistic models communicate must be considered. Third, the way that the atomistic model is terminated can be important. Finally, one must decide how much of the dislocated crystal must be included in the atomistic simulation cell.

For an elastically isotropic body, the displacement fields for screw and edge dislocations are given by Equations 1 and 2, respectively. However, most minerals are not elastically isotropic and to avoid a discontinuity between the elastic and atomistic parts of the model the correct, anisotropic solution is required. In the general case with 21 independent elastic constants analytical solutions are not available, even given the symmetry afforded by the straight dislocation line (Steeds and Willis, 1979). However, several approaches to the anisotropic problem have been suggested (Stroth, 1958; Hirth, 1972; Asaro *et al.*, 1973) most notably using the crystal's symmetry to simplify the problem to one that can be solved analytically (Steeds, 1973). The effect of limited anisotropy of the sort that can be handled analytically is shown in Figure 4. This compares the displacement field for a screw dislocation in an elastically isotropic body with one in an anisotropic body where the symmetry of the elastic constants tensor compatible with the dislocation line being aligned along a

2-fold rotation axis with a second 2-fold rotation axis perpendicular to the dislocation line. An example of this symmetry is found in orthorhombic crystals with the dislocation line aligned parallel with one of the lattice vectors, for example. In this case the effect of the anisotropy is simply to change the pitch of the screw dislocation from a situation in the isotropic case where it is independent of the angle around the dislocation line to one where a steep pitch is found in directions where the shear modulus is soft and shallow in directions where the modulus is stiff. The use analytical solutions for the displacement field in elastically anisotropic minerals was one of the ingredients in the approach described by Walker et al. (2005a), but this is not a fully general solution.

Numerical approaches to finding the elastic displacements field in the the general case are possible and two are described in Hirth and Lothe (1982). The first of these, the sextic theory (Stroth, 1958), has been used to provide an illustration of some of the key concepts. We don't fully describe the computational steps used to derive these solutions here but, briefly, the approach involves finding the roots of a sixth-order polynomial. The seven coefficients of the polynomial are combinations of elements of the elastic constants tensor. The complex roots are then used with the components of the Burgers vector to form a set of six simultaneous equations. The real parts of the solutions to these equations are summed to yield the elastic displacement field, while the imaginary parts give the anisotropic energy factor, K. The effect of general anisotropy can be seen in Figure 5 where this numerical approach has been used to find the displacement field for a screw dislocation in a triclinic crystal with exaggerated anisotropy. The major effect is due to the existence of cross terms in the elastic constants tensor which act to include edge dislocation like displacements perpendicular to the dislocation line in the displacement field of the screw dislocation. The use of this numerical approach makes it possible to model the core of dislocations in minerals of any symmetry, as well as opening the possibility of describing mixed dislocations and dislocations which do not align with symmetry elements in the higher symmetry crystals.

The second issue relates to how the elastic and atomistic segments of the model communicate; how forces between atoms cross the model divide. These forces arise from changes in the structure of the core: rearrangement of the atoms inside the core will mean that the surrounding atoms will change the relative positions of atoms inside and outside the core, leading to forces on the external atoms. One way to visualise this is to consider the effect of the atoms inside the core moving away from each other as they relax from their initial configuration to an energy minimum configuration. This will generate an outward force on the surrounding atoms as the volume of the core increases. The result is an additional 'core displacement field' surrounding the dislocation core that is not anticipated in the linear elastic Volterra solution. The question is how should this force and the

resulting displacements be handled? The problem has been intensively studied in the materials science literature since some of the earliest computational work modelling dislocations was performed on metals. Various boundary conditions were developed to account for the behaviour of the crystal away from the dislocation core. If the core displacement field decays sufficiently rapidly that it becomes unimportant before reaching the edge of the relaxed part of the simulation cell, then rigid boundary conditions, where the outer atoms are held fixed in the location predicated by linear elasticity, can be used. Otherwise one of the flexible boundary conditions, *e.g.* Flex-I (Gehlen *et al.*, 1972), Flex-S (Sinclair, 1971) or Flex-II (Hirth, 1972; Sinclair *et al.*, 1978), must be used. Briefly, Flex-I involves calculating the forces applied on the atoms of the boundary region in order to move the atoms according to the solution of the displacements for a non-linear elastic body. These solutions are available for the isotropic case as used by Gehlen *et al*. (1972), but not for anisotropic systems. Flex-S expands the non-linear elastic displacement field as a Fourier series and splits the simulation into three regions; the forces on the middle region are used to calculate the coefficients of the expansion in order to calculate the displacements in the outer two regions. Flex-II and the more modern approach of Rao *et al*. (1998) solves the non-linear problem using Green's functions. The general feature of all of these approaches involve minimisation of the energy of the inner atomistic region then fixing this and moving the atoms that represent the elastic continuum, these two steps must be repeated until self-consistency is achieved.

With the exponential increase in the availability of computational resources and algorithmic advances in simulation methods, it has become possible to perform simulations of very large numbers of atoms using models based on parameterized interatomic models. This leads to the situation where using these efficient models it is possible to perform studies of dislocation cores in minerals using fixed boundary conditions. Indeed, thus far only fixed boundary conditions have been used for the simulation of dislocations in silicate minerals. Increasing computational resources has also lead to an increase the number of atoms that can be handled using density functional theory and an important mile-stone was reached recently when the first studies to use DFT to simulate isolated dislocations were reported (Woodward and Rao, 2002; Woodward *et al*., 2008). For these simulations the use of the flexible boundary conditions (Rao *et al*., 1998; Rao *et al*., 1999) was an essential ingredient to make the calculation feasible.

Details of exactly how the atomistic model is terminated, and how large the model has to be depend in detail on the crystal structure of the mineral being simulated. These details are discussed in the next section, but some general principles can be elucidated here. The size of the simulation cell is something that should be tested for each calculation. As discussed above, when using fixed boundary conditions the simulation cell must be large enough to contain the displacements arising

from the non-linear core effects and these extend beyond the core. Two tests for this condition are possible. One option is to plot the deviation of the final structure from the structure predicted from linear elastic theory and show that this decays within the radius of the simulation cell, before the outer boundary is reached. The second approach is to repeat the calculation with larger and larger simulation cells and seek a radius where the result becomes independent of cell radius. In practice the radius often need to be 50 Å or more implying the need to include 10^4 - 10^6 atoms in the calculations. The method of termination is also an important technical detail of simulations of dislocation cores in minerals. It is clear that whatever the method of termination, it must insulate the dislocation core from the vacuum surrounding the atomistic model otherwise the structure of the core will not correspond to that expected in an infinite system. The thickness of the outer layers must be large enough to insulate all the atoms in the inner region from the effects of the vacuum. As described below, the method of achieving this goal is dependent on how the electrostatic interactions in the model are handled.

Implementation

In realising the cluster model as a practical calculation for a mineral, the first task is to construct a correctly orientated atomistic simulation cell of the appropriate dimensions. This process begins with a standard simulation of the periodic crystal finding the positions of the atoms in the unit cell and the lattice vectors that minimise the energy. The elastic constants for the mineral are then calculated and recorded for future reference. The optimised structure is then used as input to build the simulation cell for the dislocation. By repeating the input structure in space, a simulation cell is constructed with a circular cross section approximately centred on the intended origin of the dislocation. The cell is orientated as described in Table 1 with the dislocation line aligned with the Cartesian *z* axis. The simulation cell may also need to be terminated such that it is charge neutral. For crystals which consist of charge neutral strings of atoms along the dislocation line, such as the $1/2< 1\bar{1}0 > \{110\}$ edge dislocation in MgO, this is automatically true for any termination of the simulation cell that preserves the strings of atoms. The problem is also trivial in the case of molecular crystals where there is no charge if each molecule is completely included or completely excluded from the simulation cell. For more complex crystals, charge neutrality can be achieved by trimming and manipulating the charge of atoms from the outer edge of the simulation cell so that the final cell is equivalent to the cell that would have been built from charge neutral polyhedera centred on the cations. This is exactly analogous in one dimension to the method used by Braithwaite *et al.* (2002) in their embedded-cluster study of point defects in forsterite. The exact recipe for achieving this depends on the charges assigned to the cations and the polyhederal

connectivity in the mineral. Increasingly involved examples are given in the literature for a pure-silica zeolite (Walker *et al.*, 2004), forsterite (Walker *et al*., 2005b) and wadsleyite (Walker, 2010).

The second stage of a practical cluster calculation is to introduce the dislocation into the simulation cell. Far from the core the structure will be as predicted by linear elasticity and the displacement fields described above (Figures 4 and 5) can be applied to the atoms in the simulation cell. The structure of the core is unknown so some suitable starting configuration must be selected in the hope that subsequent energy minimisation will locate the ground state structure of the core. The typical approach to simply apply the elastic displacement field to the structure of the whole dislocation, with suitable steps taken to avoid numerical instabilities at the origin. When applying this field the structure of the underlying crystal must be considered in order to avoid creating an initial structure which is beyond the scope of the potential model to correct. A pathological example would be produced if two atoms were superimposed but severe changes to the bonding can also lead to significant problems. These difficulties can be avoided by careful selection of the location of the origin of the elastic displacement field.

Once the initial structure of the simulation cell containing a dislocation has been generated the final step is to perform a geometry optimisation to find a low energy stable structure of the dislocation core. The large size of the problem requires the use of several special techniques in order for the calculation to be tractable. The choice of optimisation algorithm is important. Most efficient algorithms make use of both first and second derivatives of the energy with respect to the atomic positions. However, the $O(n^2)$ storage requirement makes the use of the full second derivative matrix impossible, even when using approximate updating schemes to avoid directly calculating elements of the Hessian. In order to avoid the large increase in number of required energy evaluations implied by turning to a first-derivatives only optimiser the use of limited memory Hessian methods are useful. Specifically, the use of the limited memory BFGS approach implemented in the GULP code has proved useful (Nocedal 1980; Gale and Rohl 2003). The second important consideration, beyond minimising the number of energy evaluations, is reducing cost of each energy evaluation. For an interatomic potential model of a large system the cost of the energy evaluation is dominated by the evaluation of the electrostatic energy and so care must be taken when calculating this term. In contrast with the two or three dimensional cases, there is no problem in principle with the calculation in one dimension, the 1D Coulomb summation is absolutely, if slowly, convergent (Gale and Rohl, 2003). However, the slow convergence makes a simple real space summation inappropriate for these terms. Several methods are now available which make the problem tractable and in recent studies approaches due to Saunders *et al.* (1994) and Wolf *et al.* (1999) have been used. Both have been implemented in recent versions of the

GULP code (Gale and Rohl, 2003). For cells with a smaller radius a summation originally developed for the simulation of polymers is convenient (Saunders *et al.*, 1994). This approach is based on the Euler-MacLaurin summation formula and involves the application of a neutralising background for each ion in the system. As the cell radius increases, this scheme becomes increasingly inefficient. A faster approach for these large cells is a real-space Coulomb sum (Wolf *et al.*, 1999). This has the advantage of allowing domain decomposition and thus linear scaling with the number of atoms in the simulation cell. However, the short range part of the potential model needs to be be refitted when the Wolf summation is used.

Extracting the dislocation energy and structure

The energy minimisation procedure yields a structure of the dislocation core. Further steps are needed to evaluate the energy associated with the formation of the core and to interpret the structure. The calculated energy of the simulation cell contains a core term and an elastic term that varies with radius, as described by Equation 4. Extracting the core energy and radius requires additional calculations. The first step is to evaluate total energy stored by the dislocation (the difference between the energy of the cell containing the dislocation and an equivalent cell without the dislocation) inside a series of radii smaller then the radius of the simulation cell. In order do this for each particular radius the final atomistic model is divided into two parts. Region I contains all atoms found closer to the origin than the chosen radius while the remaining atoms are assigned to region II. The energy of the simulation cell containing the dislocation is then partitioned into interactions between atoms within region I, interactions between atoms in region II, and interactions between the two regions. The energy of the perfect cell is then partitioned in the same way while ensuring the distribution of atoms between the two regions is identical. The energy stored by the dislocation within the cut-off radius is then given by the difference between the energies of region I of the perfect and dislocated cell, including the interaction energy between region I and II. Figure 6a shows the energy calculated in this way for a screw dislocation in wadsleyite (solid points) fitted to Equation 4 (shown by the line). The logarithmic relationship between energy and radius is particularly clear when using the log-radius scale shown in Figure 6b where the deviation from the fitted line at small radii is a reflection of the core energy. However, the fitting procedure does not yield a unique solution for the dislocation core radius and core energy as these two parameters are correlated. An alternative approach to finding the core energy is illustrated in Figure 6c where the difference between the elastic and calculated energies are plotted as a function of radius (Clouet, 2009). This graph (Figure 6c) converges on the core energy at large radii and the core radius can then be directly read from Figure 6b using the core energy.

The dislocation structure can be analysed in a number of ways and on several length-scales. On the smallest scale it is possible to use the atomic positions to gain an understanding of the bonding in the core which can be directly compared with the perfect mineral structure. On a longer length-scale a useful comparison is between the structure predicted from linear elasticity and that resulting from the atomic scale simulation. Although changes in this measure close to the origin have limited relevance as the initial structure is rather arbitrary, away from the core this measure is a direct way to probe the deformation caused by changes in the size or shape of the core and non-linear elastic effects.

Dipole models

The second distinct approach to modelling dislocation cores is to build an array of dislocations so that a periodic simulation cell can be constructed. Forcing the dislocation into a periodic model has the advantage of allowing the simulation to be performed using any of the common simulation techniques used in computational mineral physics. For example, density functional theory calculations are commonly performed using a plane-wave basis set, where fully periodic boundary conditions are essential. The first difficulty with this approach is that a simulation cell containing a single dislocation cannot fit within periodic boundary conditions. At least two dislocation are needed in each simulation cell such that the sum of the Burgers vectors is zero and a dislocation dipole is formed (Figure 7). For this reason the approach is often known as the dipole method. The second difficulty is in common with similar super-cell calculations for point defects. Rather than simulating an isolated point defect or dislocation, an infinite array of defects are simulated and adjacent defects can interact, changing the defect structure and properties. These defect-defect or dislocation-dislocation interactions must be understood and minimised if any super-cell approach is to yield useful results. It is worth noting that, with the exception of some studies of diamond that are described below, this type of calculation has not yet been pursued in the mineral sciences and much of the discussion comes from the materials and physics literature.

Dislocation-dislocation interactions

The origin of major interactions between dislocations is elastic. Beyond the necessity to ensure that the system is periodic (by making the sum of the Burgers vectors zero) one must also take care that the superposition of the elastic stress fields produces no net force on any of the dislocations (e.g. Woodward, 2005). If this condition is not fulfilled, there will be a spurious interaction force in the simulation which will tend to cause the dislocation to move during dynamics or energy minimisation. Furthermore, it is necessary to ensure that the array of dislocations do not result in the formation of unintended misfit across the cell boundaries. This was a problem with some early

simulations of dislocations in silicon, identified and resolved by Bigger *et al*. (1992) who showed that it is necessary to introduce a quadrupolar rather than dipolar lattice of dislocations.

Although the correct arrangement of the dislocations in the simulation cell allows the structure of the dislocation core to be determined, finding the energy is less straightforward. There is an elastic interaction energy between the dislocations in the simulation cell and their periodic images that must be subtracted from the total energy of the cell. The difficulty is that the summation is conditionally convergent and special techniques must be used to properly obtain the correction energy (Cai *et al*. 2001; 2003). There is also an elastic interaction energy between the two dislocations within the central simulation cell that must be corrected and removed. Finally, in order to allow rigourous comparisons with cluster calculations, it is necessary to include a correction for the core traction term (Clouet, 2009).

Using the dipole approach, the dislocation structure and formation energy can be calculated given a sufficiently large simulation cell and the core energy can be found from the variation in the total energy of the simulation cell with cell size. Examples of the sort of calculation that can be undertaken using this approach include studies of molybdenum and tantalum (Ismail-Beigi and Arias, 2000), of semiconductors (Bigger *et al.*, 1992; Liu *et al.*, 1995; Heggie *et al.*, 2000; Kaplan *et al.*, 2000; Cai *et al.*, 2001) and of diamond and graphite (Heggie *et al.*, 2000; Ewels *et al.*, 2001; Heggie *et al.*, 2002; Martsinovich *et al.*, 2003; Suarez-Martinez *et al.* 2007). To our knowledge, the series of studies of dislocations in diamond and graphite represent the only examples of super-cells being used for the study of dislocations in minerals. This work also made use of fully aperiodic (e.g. Heggie *et al.*, 2000) and 1D periodic cluster based models (Blumenau *et al.*, 2002) to investigate a wide range of dislocation properties using DFT and tight-binding methods. Key results include the identification of the mechanisms of graphitization (Ewels *et al.*, 2001) and hydrogen-facilitated kink mobility (Heggie *et al.*, 2002) in diamond. An interesting effect of imposing periodic boundary conditions has been described recently in a study of dislocations in iron. Clouet *et al*. (2009) examined the variation of simulation cell energy with cell size for three arrangements of 1/2<111> screw dislocations in bcc iron using DFT and showed that the predicted core energy (after correcting for the elastic interactions) were different. The reason for this was that for all of their simulation cells (of up to ~350 atoms) the dislocation cores were sufficiently close together that non-linear elastic interactions between dislocations were important. After correcting for these terms, Clouet *et al.* (2009) were able to extract constant values for the core energy from their simulations.

Peierls-Nabarro model

The third major class of models that can be used to find the atomic scale structure and properties of the dislocation core involve seeking a simplified description of a dislocation. The simplification,

first introduced and refined by Peierls (1940) and Nabarro (1947), leads to a description of dislocations including an effective core, without having to explicitly treat the atomic scale details. In essence, this is a continuum model of a dislocation including a core. The key to this Peierls-Nabarro (PN) model is that the model dislocated crystal is constructed in a different way to approaches based on the symmetry of the Volterra dislocation. Instead of considering the crystal as a single elastic body, it is separated into two elastic half crystals, one above and one below the the glide plane, as shown in Figure 8a. The dislocation is then considered as a distribution of mismatch across the glide plane shown in Figure 8b. The derivative of the mismatch function, expressed as the 'local dislocation density', is a measure of the localisation of the dislocation core on the glide plane. For a single dislocation the mismatch function must fulfil the boundary conditions:

$$\lim_{x\to-\infty} S(x) = 0; \lim_{x\to\infty} S(x) = b \tag{5}$$

The approach is to consider the forces acting on a plane of atoms above (A) and below (B) the glide plane. The forces on each plane arise from two origins. First is the elastic response of the half-crystal containing the plane of atoms which is given as a shear stress, τ, on the plane by:

$$\tau = \frac{\mu}{\pi(1-\nu)} \int_{-\infty}^{\infty} \frac{1}{x'-x} \frac{du}{dx} dx' \tag{6}$$

for an elastically isotropic system (Nabarro, 1947). This stress will tend to keep the separation of the atoms within the plane constant and thus spread the mismatch function out, extending the dislocation core. If this were the only force the dislocation would be equally distributed across the entire glide plane and the mismatch function would increase monotonically giving a constant infinitesimal local dislocation density. The second force acts across the glide plane and acts to keep the atoms in plane A and plane B aligned, minimising the mismatch. Because the forces between atoms are balanced at equilibrium, this non-elastic interaction force must disappear for zero mismatch and mismatch giving a displacement equal to the Burgers vector, where the crystal's translational symmetry returns the system to an equilibrium configuration. Peierls (1940) assumed the interaction force was a sinusoidal function of the offset across the glide plane and parameterized the function to match the elastic modulus of the crystal for small displacements giving:

$$\tau = \frac{-\mu}{2\pi} \sin \frac{2\pi S(x)}{a} \tag{7}$$

As the non-elastic force becomes more important the dislocation becomes more localised to the centre of the glide plane. At equilibrium the stresses described by Equations 6 and 7 balance, leading to the Peierls Nabarro equation:

$$\int_{-\infty}^{+\infty} \frac{1}{x-x'}\left[\frac{dS(x')}{dx'}\right] dx' = (1-\nu)\sin\frac{2\pi S(x)}{a} \tag{8}$$

Which has the the solution:

$$\frac{S(x)}{b} = \frac{1}{2} + \frac{1}{\pi}\arctan\frac{2x(1-\nu)}{a} \tag{9}$$

Figure 9 shows the mismatch function and local dislocation density distribution for three different values of Poisson's ratio calculated using this model. The size of the dislocation can be characterised by a half-width, the region where the value of $S(x)$ is more than half its maximum. This width is given by $a/\{2(1-\nu)\}$ or, more generally, $Kb/(4\pi\tau_{max})$. Increasing Poisson's ratio spreads the dislocation out more on the glide plane and is equivalent to increasing the size of the elastic force at the expense of the force acting across the interface.

DFT and the GSF

In order to understand how the PN model is used with modern atomic scale simulation, it is necessary to first consider the concept of the generalised stacking fault, or GSF. The idea, first introduced by Vítek (1968) in the context of the exploration of stacking faults in bcc metals, is that the atomistic interaction energy across a shear plane can be mapped out constructing a "γ surface" showing the energy as a function of displacement. The approach is to define a plane in a model crystal, displace one half of the crystal relative to the other half and relax the structure normal to the shear plane while constraining the calculation to preserve the displacement and localise it on the chosen plane. This gives an energy associated with the chosen displacement and the procedure is repeated for the all displacements on the plane within the unit cell. It is because any displacement can be chosen the stacking faults are described as 'generalised' (Christian and Vítek, 1970). Each structure generated in this procedure contains a stacking fault, although these will mostly be unstable and are associated with a restoring force equal to the negative of the energy gradient in the direction of displacement. When the GSF contains a single maximum no stacking fault is stable in this plane: stable stacking faults are represented by metastable energy minima. The gradient of the GSF is related to the strength of the perfect crystal; a resolved shear stress greater than the maximum gradient is sufficient to cause a perfect, defect-free crystal to deform by shearing along that plane. The maximum gradient is known as the ideal shear stress or ISS and this first point of

contact between the GSF and deformation can directly provide useful information (e.g. Li *et al*., 2003).

The close relationship between the GSF and the PN model was pointed out by Christian and Vítek (1970), who showed that the sinusoidal function assumed by Peierls (1940) and Nabarro (1947) to represent the restoring force (Equation 7) could, in principle, be replaced by the negative of the derivative of the stacking fault energy with respect to displacement of the two planes of atoms. This approach was quickly refined and used for bcc metals using stacking fault energies from inter-atomic potentials (Lejček, 1972; Kroupa and Lejček, 1972). By the 1990s it was possible to calculate the stacking fault energies using DFT and use these to solve the PN model for silicon (Joós *et al*., 1994) and a wide range of other materials including Al (Sun and Kaxiras, 1997; Hartford *et al*., 1998), Pd (Hartford *et al*., 1998), NiAl and FeAl (Medvedeva *et al*., 1996), TiAl and CuAu (Mryasov *et al*., 1998), Si (Kaxiras and Duesbery, 1993; Joos *et al*., 1994; de Koning *et al*., 1998) and MgO (Miranda and Scandolo, 2005). The approach of Joós *et al*. (1994) was eventually adopted for the study of minerals as described in detail in a study of ringwoodite (Carrez *et al*., 2006). In this approach the integrodifferential PN equation is written as:

$$\frac{K}{2\pi}\int_{-\infty}^{+\infty}\frac{1}{x-x'}\left[\frac{dS(x')}{dx'}\right]dx' = F(S(x)) \tag{10}$$

where the the sinusoidal restoring force on the right hand side of Equation 8 has been replaced with an unknown restoring force that is itself a function of the mismatch and elastic anisotropy has been assumed. The solution for the mismatch function is assumed to take the form:

$$S(x) = \frac{b}{2} + \frac{b}{\pi}\sum_{i=1}^{N}\alpha_i \arctan\frac{x-x_i}{c_i} \tag{11}$$

where α_i, x_i and c_i are variational constants, N is an integer controlling total number of variables and the normalization condition leads to:

$$\sum_{i=1}^{N}\alpha_i = 1 \tag{12}$$

with each α_i a positive number. Substituting Equation 11 into the left hand side of Equation 10 gives the trial solution for the PN equation:

$$F(x) = \frac{Kb}{2\pi}\sum_{i=1}^{N}\alpha_i\frac{c_i}{(x-x_i)^2+c_i^2} \tag{13}$$

Varying the constants to minimising the difference between the restoring force predicted from the GSF calculation and those predicted by Equation 13 leads to a solution for the mismatch function. Practically, the variational constants α_i, x_i and c_i are found obtained from least-squared minimisation of the difference between Equation 13 and the forces obtained from the atomic scale GSF calculations. Differentiation of the mismatch function gives the profile of the density of partial dislocations across the glide plane, exactly as shown in Figure 9.

To summarise, the PN model involves describing the dislocated crystal as consisting of two parts separated by the glide plane and each described by linear elasticity. A non-elastic force is assumed to operate between the two half-crystals across the glide plane. By imposing boundary conditions that imply the presence of a dislocation and balancing the elastic and non-elastic forces, the profile of the dislocation can be found. Both the elastic and non-elastic forces can be found by tractable calculations based on density functional theory making the approach attractive for predictive calculations. Key approximations are that the dislocation core is limited to a single (chosen) glide plane, that any partial dislocations are collinear, and that the deformation of the crystal slightly away from the glide plane, even within the core, can be described using linear elasticity. Some of the consequences of these approximations will be illustrated below, along with emerging ways that can be used to relax the approximations (e.g. Bulatov and Kaxiras, 1997; Lu, 2005; Schoeck, 1999a; 2005; Schoeck and Krystian, 2005).

Recovering an atomic scale description

In the construction of the PN model the atomic structure of the dislocation is discarded. This makes direct comparison with the dipole and cluster approaches difficult and introduces a significant problem: just like an elastic Volterra type model of a dislocation, a PN dislocation experiences no resistance to movement. Selecting a different origin on the *x*-axis, corresponding to moving the dislocation does not alter the PN solution. In order to study the resistance to motion of the dislocation, or examine the core structure, it is necessary to reintroduce the atomic structure (Joós *et al*., 1994; Schoeck, 1999b). The key to achieving this is the construction of a misfit energy. This energy is a function of the core displacement, *u*, and is given summing the misfit energies between pairs of atomic planes. The misfit between planes is given by $S(ma'-u)$, where *m* the number of planes from the origin, a' is the inter-planar distance and *S* is the disregistry function generated from the PN model. Multiplying this mismatch by the GSF energy gives the contribution of this plane to the misfit energy and summing over all planes gives the energy cost of displacing the dislocation:

$$W(u) = \sum_{i=-\infty}^{+\infty} \gamma(S(ma' - u))a' \qquad (14)$$

The Peierls stress is then found by seeking the maximum derivative of the misfit energy with respect to the displacement of the dislocation core:

$$\sigma_p = \max\left\{\frac{1}{b}\frac{dW(u)}{du}\right\} \tag{15}$$

For visualisation and comparison with the dipole and cluster approaches it is useful to be able to generate an atomic scale representation corresponding to the solution to the PN model. The approach is to start with a atomic scale model of the crystal, displace the atoms above the glide plane according to the calculated disregistry function, then applying the elastic displacement field for the local dislocation density distribution also taken from the PN model (Carrez *et al*., 2007a). For an edge dislocation these displacements are given by:

$$\begin{aligned} u_x &= \frac{1}{2\pi}\int_{-\infty}^{+\infty}\left[\arctan\left(\frac{y}{x-x'}\right)+\frac{(x-x')y}{2(1-\nu)\left((x-x')^2+y^2\right)}\right]\rho(x')dx' \\ u_y &= -\frac{1}{2\pi}\int_{-\infty}^{+\infty}\left[\frac{1-2\nu}{4(1-\nu)}\ln\left((x-x')^2+y^2\right)+\frac{(x-x')^2-y^2}{4(1-\nu)\left((x-x')^2+y^2\right)}\right]\rho(x')dx' \\ u_z &= 0 \end{aligned} \tag{16}$$

which can be directly compared with equation 2 and where isotropic elasticity has been assumed.

Periclase, halite and related materials

Rock salt structured (B1) minerals such as halite (NaCl) and periclase (MgO) have been used as a structurally simple tests for many developing areas of computational mineral science. Studies of dislocation cores are no exception with much of the early work focusing on this type of material. Some of the earliest work includes an investigation of the core structure and Peierls stress of dislocations in alkali halides using a cluster based approach (Hoagland *et al.*, 1976) and a series of studies undertaken by Puls and co-workers leading to the development of the PDINT code for the cluster-based simulation of dislocations in cubic ionic materials. Concentrating on MgO as a model system this group first used a simple shell model with ridged boundary conditions to calculate the Peierls energy for the 1/2$<1\bar{1}0>\{110\}$ edge dislocation (Puls and Norgett, 1976; Woo and Puls, 1976). A breathing shell model was then used with the Flex-II boundary conditions to recalculate the geometry of the dislocation core (Woo and Puls, 1977a) and to re-evaluate the Peierls energy barrier (Woo and Puls, 1977b). The code was then developed further in order to model point defect – line defect interactions, again in MgO (Puls *et al.*, 1977; Puls, 1980, 1983). Further work involved comparisons between the behaviour of MgO, NaCl and NiO (Rabier and Puls, 1989; Rabier *et al.*, 1990). These studies were somewhat limited by the relatively small number of atoms

that could be included in the simulation cell and utilised a Coulomb summation scheme that could only handle cases where charge-neutral strings of atoms were aligned parallel to the dislocation line. More recent work by Watson and co-workers began to address these issues. This group, using the METADISE code (Watson *et al.*, 1996), were able to study screw dislocations in MgO (Watson *et al.*, 1999) and the effect of these dislocations on the MgO {100} surface (Watson *et al.*, 2001). A key development was the use of a Coulomb sum that can handle the general case.

We can usefully compare the Peierls stress calculated from the different cluster based models (Woo and Puls, 1977b) of the $1/2<1\bar{1}0>\{110\}$ edge dislocation MgO with those more recently calculated using the Peierls-Nabarro model (Carrez *et al.*, 2009a) which gives a core structure shown in Figure 10. This is the stress required to move a straight dislocation line in the direction of the Burgers vector over the energy barrier imposed by the periodic crystal structure (the Peierls barrier) without generating kinks. When resolved onto the glide plane, this stress is sufficient to move the dislocation through an otherwise perfect crystal at zero K. The cluster based methods (Woo and Puls, 1977b) give the height of the Peierls barrier as between 1.4×10^{-3} and 0.8×10^{-3} eV/Å, depending on which inter-atomic potential is used (Table 2) while the PN approach, which utilises density functional theory, gives a barrier height of 0.03×10^{-3} eV/Å. This variation leads to a difference in the predicted Peierls stress, which is 20 MPa for the PN model and between 46 and 76 MPa for the cluster based calculations (Table 2). The reason for this discrepancy is unclear. One possibility is that the relatively small size of the cluster based calculations leads to an overestimate of the energy barrier. It is also possible that the use of formal charges on the ions in these models causes the overestimate in barrier height (formal charge models can overestimate energy barriers for point defect diffusion, Walker *et al.* 2003). Alternatively, the PN model could underestimate the Peierls barrier and stress, perhaps by underestimating the difference in structure between a dislocation in its minimum and maximum energy configuration. This possibility is discussed in more detail with regards to forsterite below.

Dislocations in perovskite and post-perovskite structured minerals

One of the key reasons for modelling the cores of dislocations is the ability to predict the rate and style of the deformation of mantle minerals in order to better constrain the dynamics of the Earth's interior and understand the origin of plate tectonics. In the case of lower mantle perovskite and the recently discovered post-perovskite phase (Murakami *et al*., 2004; Oganov and Ono, 2004; Tsuchiya *et al*., 2004; Iitaka *et al*., 2004) such predictions are particularly useful. Experiments examining the deformation behaviour of these minerals are difficult; large-volume deformation apparatus is currently limited to ~15 GPa (Yamazaki and Karato, 2001; Wang *et al*., 2003) and although deformation experiments are possible in the diamond anvil cell (e.g. Kinsland and Basset,

1977; Merkel *et al*., 2007; Miyagi *et al*., 2009) they are beset by problems with small sample sizes, high stresses, and difficulties in reaching high temperature. While developments are ongoing to enhance the ability to perform high pressure deformation experiments, an ability to predict the strength of lower mantle minerals and thus the viscosity of the Earth is clearly useful. A second fundamental problem with experimental studies is that recovered samples of $MgSiO_3$ perovskite are unstable in electron beam of the TEM and many materials, such as $MgSiO_3$ post-perovskite, low spin ferropericlase and $CaSiO_3$ perovskite, cannot be recovered to ambient conditions. Because of these difficulties, much of the experimental work on the deformation of lower mantle minerals has been performed on analogue materials which are stable at much lower pressure (e.g. Wright *et al*., 1992; Li *et al*., 1996; Miyagi *et al*., 2008; Miyajima and Walte, 2009).

Perovskites

The perovskite structure is common and accepts a wide range of chemistry. It consists of a large 12 coordinate cation 'A' site and an octahedral 'B' site. The B site octahedra are corner sharing and the anions are arranged in a face-centred cubic lattice. The idealised structure is cubic and is illustrated by tausonite ($SrTiO_3$) in Figure 11a. If the 'A' cations are too small, the symmetry can easily be lowered (tetragonal, orthorhombic) by tilting the octahedra relative to each other. This is the case for the mineral perovskite ($CaTiO_3$) which is orthorhombic and hence does not exhibit the ideal perovskite structure. The structural flexibility leads to the wide range of possible compounds and minerals that can form with this structure. $MgSiO_3$ perovskite shown in Figure 11b is of direct interest in studies of the deep Earth, as (with some Al and Fe) it forms 80% of the lower mantle, by volume. In common with $CaTiO_3$, this structure is distorted to orthorhombic symmetry. $CaSiO_3$ perovskite represents a smaller fraction of the average lower mantle (7% by weight) but it is much more abundant (20 weight %) in subducted slabs. $CaSiO_3$ perovskite has cubic, or almost cubic, symmetry. All four of these materials have been the subject of dislocation modelling using the Peierls-Nabarro model with generalised stacking fault line energies calculated within DFT using a plane-wave basis for the valence electrons and the projector augmented-wave method to describe the core electrons (Ferré *et al.*, 2007; Carrez *et al.*, 2007a; Ferré *et al.*, 2008; 2009a; 2009b). $SrTiO_3$ represents an interesting case since, thanks to its industrial applications, it has been the subject of numerous experimental studies. In particular, the core structure of dislocations in $SrTiO_3$ has recently been the subject of very detailed studies using HRTEM (Jia *et al*., 2005) and EELS (Zhang *et al.*, 2002a; 2002b) leading to atomic-scale models of dislocation cores that can be compared to PN models. Jia *et al*. (2005) have used Cs correction together with numerical phase-retrieval techniques to image the dislocation core of an <100>{011} dislocation in $SrTiO_3$. Using the PN model to produce an atomic structure of the same dislocation, Ferré *et al*. (2008) have shown that the essential elements of the core structure were satisfactorily reproduced by the model. This was

the first validation of the method with a complex oxide. In this study, four potential slip systems were compared: <100>{010}, <100>{011}, <110>{001} and <110>{1$\bar{1}$0}. The GSF corresponding to <110>{1$\bar{1}$0} is very flat and results in a widely spread dislocation core which bears little lattice friction. Indeed, this correspond to the easiest slip system as observed in experimental studies (e.g. Nishigaki *et al*., 1991; Matsunaga and Saka, 2000; Brunner *et al*. 2001; Gumbsch *et al*., 2001). For the purposes of dislocation core modelling, $CaSiO_3$ was assumed to be cubic (Ferré *et al*., 2009a). Direct comparison is then possible with $SrTiO_3$. Since $CaSiO_3$ perovskite is stable throughout the whole lower mantle, three pressures were considered 0, 30 and 100 GPa. At 0 GPa, $SrTiO_3$ and $CaSiO_3$ exhibit the same essential features. The <110>{1$\bar{1}$0} GSF is flat and much lower that the others. This results in a widely spread <110>{1$\bar{1}$0} dislocation core shown in Figure 12, which glides easily. With increasing pressure, the <110>{1$\bar{1}$0} GSF in $CaSiO_3$ shows a more and more pronounced minimum at 50% shear. The dislocation core which is spread at 0 GPa, splits into two well-separated collinear partial dislocations at 30 and 100 GPa. The stacking fault between those partials correspond to edge-sharing octahedra found in the post-perovskite phase (see below). This large dissociation corresponds to a very low lattice friction, a unique case so far for a silicate under high pressure. Following earlier work and in order to compare the slip systems in the cubic and orthorhombic phases it is possible to describe the orthorhombic slip systems on the idealised cubic lattice: each of the slip cubic slip systems are split into several distinct systems by the orthorhombic distortion as shown in Table 3. In orthorhombic perovskites, PN modelling has been performed for the following slip systems: $[100]_o(010)_o$, $[100]_o(001)_o$, $[010]_o(100)_o$, $[010]_o(001)_o$, $[001]_o(100)_o$, $[001]_o(010)_o$, $[001]_o(\bar{1}10)_o$, $[\bar{1}10]_o(001)_o$ and $[110]_o(\bar{1}10)_o$ (Ferré *et al*., 2009b, see Table 3). The quasi doubling of the orthorhombic cell compared to the pseudo-cubic cell result in widely dissociated dislocations. This is the case for $[001]_o(100)_o$, $[001]_o(010)_o$, $[001]_o(\bar{1}10)_o$, $[\bar{1}10]_o(001)_o$ and $[110]_o(\bar{1}10)_o$. Slip systems which correspond to the easiest in the cubic structure, $\langle 110\rangle_c\{1\bar{1}0\}_c$, give rise to the easiest slip systems in $MgSiO_3$ perovskite as well. However the lattice friction contrast between them and the other slip systems is smaller. The reason is that orthorhombic distortions increase the stacking fault energy and result in a less extended (and thus glissile) core. The same effect is observed in $CaTiO_3$ which exhibits many features in common with $MgSiO_3$ perovskite although some differences are observed (for instance glide in $CaTiO_3$ is very easy compared to $MgSiO_3$).

Post-perovskite

One of the most dramatic recent developments in the mineral sciences was the discovery of a post-perovskite phase transition in $MgSiO_3$ at around 125 GPa and 2500 K (Murakami *et al*., 2004; Oganov and Ono, 2004; Tsuchiya *et al*., 2004, Iitaka *et al.*, 2004), corresponding to conditions found just above the core mantle boundary. A phase transition under deepest mantle conditions has long been suggested as a possible explanation for the D'' layer, a 200-300 km thick region of anomalous, heterogeneous and anisotropic seismic wave velocities observed above the core-mantle boundary. The geophysical significance of the phase transition was reviewed by Hirose (2006). The $MgSiO_3$ post-perovskite structure, shown in Figure 11c, is shared with the oxide $CaIrO_3$. It exhibits orthorhombic symmetry (space group *Cmcm*) with a = 2.456 Å, b = 8.042 Å and c = 6.093 Å (Iitaka *et al.*, 2004). The structure consists chains of edge sharing SiO_6 octahedera along the a axis which are joined by their corners to form sheets in the a-c plane. These sheets are stacked along the b axis and separated by layers of magnesium ions. The structure appears to be very anisotropic for several reason. First the unit cell has a very large aspect ratio with a being much smaller that b and c. As the elastic energy of a dislocation is proportional to the square of its Burgers vector, the aspect ratio of the unit cell is expected to have significant implications on the stabilisation of some dislocations. Second, the structure consists of octahedral layers parallel to {010}. This layering has been related (at least qualitatively) to the strong anisotropy of the D" layer (Oganov and Ono, 2004). However, Metsue *et al*. (2009) have shown that under high pressures, the bond strength contrast between Si-O and Mg-O (in the two octahedral layers) is decreased (it is much smaller than the bond strength contrast between Ca-O and Ir-O in the isostructural $CaIrO_3$, for example) and that the plastic behaviour of low pressure layered silicates cannot be simply transposed to $MgSiO_3$ post-perovskite. The elastic properties of $MgSiO_3$ post-perovskite have been calculated by several groups using DFT (see Wooky *et al*., 2005) with the conclusion that this phase transition could explain many of the seismological observations of D''. However, in order to understand the observed seismic anisotropy it is necessary to know the active deformation mechanisms. These have been probed using DFT as well as experiments on analogue materials and *in situ* deformation experiments in the diamond anvil cell (e.g. Merkel *et al*., 2006; 2007; Niwa *et al*. 2007; Hunt *et al*. 2009; Walte *et al*., 2009)

Metadynamics calculations using DFT allowed Oganov *et al*. (2005) to probe the perovskite to post-perovskite transition mechanism. These calculations suggested that the transition was accomplished by shear and the formation of stacking faults leading to a lattice preferred orientation (LPO) dominated by {110} planes. Deformation has been examined by applying the PN model to several potential slip systems of the post-perovskite structured $MgGeO_3$, $CaIrO_3$ and $MgSiO_3$: [100](010), [100](001), [100](011), [001](010), [001](110), [001](100), [010](100), [010](001), ½[110](001) and ½[110]($\bar{1}$10) (Carrez *et al*., 2007a; 2007b; Metsue *et al.,* 2009). The additional

½[110] Burgers vectors arose from consideration of the *Cmcm* space group, which is face centred. The occurrence of a very small lattice distance *a* has several implications on the dislocation structures and properties. It tends to stabilise [100] dislocations which exhibit the lowest elastic energy. However, these dislocations will have to glide over the longest distance, *b* and *c*. The PN model shows that lattice friction is very sensitive to the translation vector. Another implication is that dislocations with a high elastic energy, such as screw [010](001) dislocations that move along [100], will see a decrease of their lattice friction. The core of [100] dislocations is very narrow which does not favour their mobility. ½[110] dislocation exhibit quite similar core profiles to [100], although they are slightly wider. In case of [001] and [010] dislocations, the PN model shows that the higher elastic energy can be relaxed by significant dissociation into two or three (e.g. [010](100)) partial dislocations as shown in Figure 13. As a result, [100](001) exhibits the lowest lattice friction in $MgGeO_3$ post-perovskite (surprisingly, the easy glide plane is not in the (010) octahedral layers). This is not the case in $MgSiO_3$ and $CaIrO_3$ where glide is easier along [001](010). Metsue *et al.* (2009) have shown that such differences are observed between those three compounds although the dislocations exhibit generally the same structures. These calculations showed that the [001](010) slip system is the weakest and will thus accommodate most of the strain in dislocation controlled deformation leading to a (010) type LPO. To further quantify differences in the LPO, Metsue *et al.* (2009) used their results to perform VPSC calculations and find the expected texture of polycrystalline samples deforming via dislocation glide. The $CaIrO_3$ and $MgSiO_3$ post-perovskite phases produced virtually identical distributions of crystal orientations, while $MgGeO_3$ produced a different distribution of orientations.

Forsterite, wadsleyite and ringwoodite

The upper mantle and transition zone, to a depth of 660 km, is dominated by the three Mg_2SiO_4 phases olivine (to ~440 km), wadsleyite (~440-520 km), and ringwoodite (to 660 km). Despite the fact that deformation experiments are possible under upper mantle conditions, the deformation mechanisms controlling the rheology of these phases, and thus the the upper mantle, remains an open question. In the upper part of the upper mantle, seismic anisotropy is consistent with deformation dominated by the glide of [100] dislocations in olivine. But the observed anisotropy changes at higher pressure and around subduction zones, observations that has lead to a wide range of hypotheses spanning corner flow in the mantle wedge (Russo and Silver, 1994), changes in the active slip system in olivine caused by pressure (Couvy *et al.*, 2004; Raterron *et al.*, 2007; 2009; Jung *et al.*, 2009) or water content (Jung and Karato, 2001; Katayma and Karato, 2006; 2008; Jung et al. 2006), and an upper mantle anisotropy dominated by the presence of hydrous layer silicates (Katayama *et al.*, 2009; Healy et al. 2009). The situation in the transition zone is perhaps even more

confused, but reliable data on deformation mechanisms in this region offer the prize of understanding how mantle flow responds to the rapid increase in viscosity in this region.

Apart from MgO, forsterite was the first mantle mineral where dislocation cores have been studied at the atomic scale. Both the cluster and PN approaches have been used and many of the complications of using these methods for complex minerals were first addressed in these early studies (Walker *et al*., 2005b; Durinck *et al*., 2007). There has also been a detailed comparison between results from the two approaches, which provides a useful illustration of their relative strengths and weaknesses (Carrez *et al*. 2008). More recently attention has turned to wadsleyite, which has also been studied using the PN and cluster approaches (Metsue *et al*. 2010; Walker 2010). Ringwoodite was the subject of one of the early PN studies of mantle minerals, which provides a good example of this approach (Carrez *et al*., 2006).

Cluster based models of dislocation cores in forsterite concentrated on the two common screw dislocations with [100] and [001] Burgers vectors and made use of fixed boundary conditions and the advances reviewed above (Walker *et al*., 2005a; 2005b). Analysis of the structure concentrated on the atomic scale reconstruction in the dislocation core and on the non-Volterra displacement field extending from the core. The magnitude of the Burgers vector for these two dislocations is similar (~4.7 and ~6.0 Å for [100] and [001], respectively) and the elastic shear anisotropy is small (c_{44} is about 17% smaller than c_{66}), so differences in the properties of the two dislocations are likely to be due to the structure of the core. In both cases the non-Volterra displacements were found to be inwards, towards the core, but the size of this effect is larger for the [100] than the [001] dislocation. The reason for this difference seems to be that magnesium ions closest to the core of the [001] screw dislocation are able to maintain octahederal coordination while those in the core of the [100] screw dislocation are not and form a more distorted but lower volume structure.

The PN modelling of dislocations in forsterite was used to study both edge and screw dislocations and to probe the influence of pressure on the various dislocations. The first studies involved calculating the GSF energies (Durinck *et al.*, 2005a) and examining how these changed with pressure (Durnick *et al*., 2005b). Key results from this early work were that GSFs corresponding to easy slip systems in experiment yielded the lowest ideal shear stress and that pressure significantly lowered the ideal shear stress for slip systems with a [100] Burgers vector while those with [001] Burgers vectors were less effected. This result helped explain emerging experimental findings that suggested that the dominant slip system (i.e. the hardest slip system that contributed to plastic deformation) changed from [100](010) to [001](010) with increasing pressure (Couvy *et al.*, 2004). The findings from the ideal shear strength calculations were essentially confirmed when the GSF energies were used to parameterize the PN model (Durinck *et al*., 2007). It was noted that screw

dislocations were always less mobile than edge dislocations in forsterite (Durinck et al. 2007). An additional result was that the [001] dislocations spread in the (100) and {110} planes in the PN model, but the [100] dislocations tended to yield a narrow core in all slip planes. On the basis of this observation, Durinck *et al*. (2007) suggested that the [001] screw dislocation may have a complex non-planar core structure and that this could explain experimental observations that [001] screw dislocation segments are typically long and straight.

The suggestion of a non-planar core structure for [001] screw dislocations in forsterite motivated a comparison of the core structure predicted by Walker *et al*. (2005b) using a cluster model and Durinck *et al*. (2007) using the PN model (Carrez *et al*., 2008). The first potential difficulty with this comparison was that the underlying method used to describe the interactions between atoms was different in the two cases: density functional theory was used for the PN model while parameterized interatomic potentials were used for the cluster model. This was addressed by recalculating the relevant GSF energies using the same interatomic potential used by Walker *et al*.(2005b). The resulting PN models were qualitatively similar to those of Durinck *et al*. (2007) although the maximum of the GSF, and thus the ISS, was higher for the potentials than for the DFT results. With major differences due to the choice of atomic interaction ruled out the next stage was to visualise the difference in the structure predicted by the two methods using the differential displacement, or Vítek representation (Vítek e*t al.*, 1970) illustrated in Figure 14. Comparing the two structures, which are shown in Figure 15, is instructive as it illustrates the major differences between the cluster and PN methods. The difference in the structures also suggests a mechanism for the formation of the long straight dislocation segments observed in experiment. The key idea comes from studies of bcc metals where it has been suggested that the core can exist in two forms, a non-planar core that is immobile under stress and a planar core which can easily move on a particular slip plane (Vítek, 1966). Movement of such a dislocation involves the formation of the planar core, which has a higher energy than the non-planar core. This can result in motion by an unlocking mechanism described by Couret and Caillard (1989) or by the formation and migration of an unstable transient core structure (Pizzagalli *et al*., 2009). The metastable planar dislocation is able to glide rapidly over a free-glide distance before it falls into its low energy stable configuration which stops glide resulting in the long dislocation segments. Initial results using the PN Galerkin model, which is described below, lend support this hypothesis.

The comparison of the structure of the [001] screw dislocation in forsterite described above highlights some of the shortcomings of the PN model. The underlying assumption is that the dislocation core only exists on one particular glide plane. Spreading and dissociation on this plane are handled by the model but not out of plane spreading or non-collinear dissociation. There are

several approaches that can be used to extend the PN model and overcome these limitations (e.g. Schoeck, 1996; 1997; Ngan, 1997; Xu and Argon, 2001) but the only approach that has been applied to the mineral sciences is the PN Galerkin (PNG) model (Denoual 2004; 2007). At its heart, the PNG model is a generalisation of the 1D PN model recast as an energy minimisation rather than a force balance problem that allows the dislocation core to spread over a number of glide planes. Instead of using analytical solutions to handle the elastic part of the PN model, an element free Galerkin approach similar to a finite element model is used. Instead of using the GSF energy directly, the elastic contribution is removed and 'inelastic stacking fault energies' are used within the code. This approach results in a method that can handle complex moving and evolving core structures with boundary conditions that can handle externally applied stress and pressure. Importantly, dislocation cores can spread onto different planes and non-collinear dissociation is possible. An early application of the PNG model has been dislocations in wadsleyite (Metsue *et al*., 2010).

The dislocation microstructure of deformed wadsleyite have been the subject of significant experimental study with eight slip systems identified as being activated by deformation (e.g. Sharp *et al*., 1994; Dupas *et al*., 1994; Dupas-Bruzek *et al*., 1998; Chen *et al*., 1998; Mossenfelder *et al*., 2000; Thurel *et al*., 2003a; Thurel and Cordier 2003; Nishihara *et al*., 2008). The elastic energy and possible dissociation schemes were analysed by Thurel *et al*. (2003b) and these authors argued that dislocations with the 1/2<111>, [010] and <101> Burgers vectors commonly dissociate into pairs of partial dislocations joined by stacking faults while dislocations with a [100] Burgers vector are generally not dissociated and commonly exhibit a screw character. The lack of dissociation of [100] dislocations and the low density of [001] dislocations is not predicted by the elastic theory. Both these observations are likely to be due to particular features of the dislocation cores, and in order to probe the structure of dislocation cores in wadsleyite Metsue *et al*. (2010) used the PNG model, with GSF energies calculated using interatomic potentials. These calculations show that 1/2<111>{101} and [100](010) are the easy slip systems at high pressure and that dislocations in both of these slip systems are dissociated. The cores of [100] and [001] screw dislocation in wadsleyite have also recently been studied using the cluster approach (Walker, 2010). These calculations reveal very different core structures for the two dislocations with the [100] core having a particularly low energy (2.5 eV/Å, Figure 6) and containing four coordinate magnesium ions. A detailed comparison of the results of the two methods has not been undertaken, principally because of the difficulty of mapping the PNG results back onto an atomic scale structure. However, there are signs that that two approaches yield similar results: the cluster approach predicts that the dislocation core spreads by about 15 Å in the [010] and [001] directions, a magnitude similar to that found from the PNG approach.

Progress and prospects

In sharp contrast to the situation only a decade ago, there are now two computational methods that have been shown to be usable for the simulation of the structure of dislocation cores in structurally complex silicate minerals. These approaches, one based on the Peierls-Nabarro model and the other involving embedding an atomistic model of the dislocation in an elastic continuum, are complementary: the Peierls-Nabarro model allows the use of predictive and ab-initio density functional theory while the cluster method is free of the approximations inherent in the PN approach. The recently described Peierls-Nabarro Galerkin model offers the opportunity to overcome some of the limitations of the original Peierls-Nabarro approach. One particular strength is the ability to model changes in complex dislocation core structures under the application of external stress. One useful direction of future research would be the development of methods to better compare the output of these two approaches, perhaps by extracting local dislocation density profiles or mismatch functions from cluster based models. In principle this should be possible given a chosen glide plane (or a set of glide planes if the comparison is with the PNG approach), but the necessary algorithm is not easy to implement. An alternative method is to decorate a PN solution with an atomic structure and compare this with the output of a cluster calculation in the manner undertaken by Carrez *et al*. (2008), but the extension of this approach to the PNG model is not completely clear.

There is also a third method that can be used to probe the properties of dislocation cores - the super-cell or dipole approach. It is not obvious why this hasn't been used to study dislocation in mantle minerals when super-cell approaches have become the dominant approach used by mineral physics for studies of point defects (e.g. Brodholt, 1997; Walker *et al*., 2007; Verma and Karki, 2009) and disordered phases (e.g. Mookherjee et al., 2008). One area where the dipole approach may prove useful is in studies of point-defect dislocation interactions. Understanding these interactions is essential to probe pipe-diffusion and dislocation climb and, usefully, the effect of dislocation - dislocation interactions should largely cancel for these processes. In many cases interatomic potentials are sufficient to probe the properties of point defects in mineral and will presumably also be sufficient to examine point-defect dislocation interactions. For example, in recent proof-of-concept calculations examining the interaction between oxygen vacancies and edge dislocations in MgO (Walker *et al*., 2009). However, when chemical bonds are broken, formed, or modified by the introduction of the point defect, or where charge transfer occurs, a simple potential model can be insufficient. In these cases the most profitable approach may be to perform the point-defect dislocation study using fully periodic boundary conditions and the dipole method to take advantage of implementations of density functional theory.

Another area ripe for exploitation is the use of models of dislocation cores to model deformation by dislocation glide. To a certain extent this information is provided by the Peierls stress which is the maximum derivative of the Peierls potential and can be extracted from the PN model (Equations 14 and 15). However, this is an upper bound on the resistance to simple dislocation glide in the absence of thermal fluctuations. At high temperature dislocation glide is expected to operate via the thermally activated nucleation of a pair of kinks. High temperatures increase the rate of kink formation while applied stress lowers the energy barrier to kink formation (Figure 16). Models exist that allow the temperature and stress dependence of kink nucleation to be found from the Peierls potential (e.g. Dorn and Rajnak, 1964; Seeger, 1981; Koizumi *et al*., 1993). Recent work on MgO by Carrez *et al*. (2009a; 2009b) has used the Peierls potential calculated using the PN model to parameterize a kink nucleation model based on balancing the kink energy with the elastic interaction between kink pairs and the work done by moving a dislocation segment (Koizumi *et al*., 1993). While this approach shows promise, extension to more complex dislocation cores may be problematic. For example, it is not clear how to apply this sort of kink nucleation model for cases such as the [001] screw dislocation in forsterite where the barrier to dislocation motion is not the Peierls barrier but the energy change associated with modifying the structure of the dislocation core.

Acknowledgements

We are grateful to a wide range of colleagues and collaborators who have provided useful discussion, guidance and support during the development of the methods and ideas described in this review. A.M.W. acknowledges the support of the NERC through a Postdoctoral Research Fellowship (NE/E012922/2).

References

Asaro, R. J., Hirth, J. P., Barnett, D. M. and Lothe, J. (1973) A further synthesis of sextic and integral theories for dislocations and line forces in anisotropic media. *Physica Status Solidi b*, **60**, 261-271.

Bigger, J. R. K., McInnes, D. A., Sutton, A. P., Payne, M. C., Stich, I., King-Smith, R. D., Bird, D. M. and Clarke, L. J. (1992) Atomic and electronic structures of the 90° partial dislocation in silicon. *Physical Review Letters*, **69**, 2224-2227.

Bilby, B. A. and Smith, E. (1956) Continuous distributions of dislocations. III. *Proceedings of the Royal Society A*, **236**, 481-505.

Bilby, B. A., Bullough, R. and Smith, E. (1955) Continuous distributions of dislocations: A new application of the methods of non-Riemannian geometry. *Proceedings of the Royal Society A*, **231**, 263-273.

Blumenau, A. T., Heggie, M. I., Fall, C. J., Jones, R. and Frauenheim, T. (2002) Dislocations in diamond: Core structures and energies. *Physical Review B*, **65**, art. num. 205205.

Braithwaite, J. S., Sushko, P. V., Wright, K. and Catlow, C. R. A. (2002) Hydrogen defects in forsterite: A test case for the embedded cluster method, *Journal of Chemical Physics*, **116**, 2628 - 2635.

Brodholt, J. P. (1997) Ab initio calculations on point defects in forsterite (Mg_2SiO_4) and implications for diffusion and creep. *American Mineralogist*, **82**, 1049-1053.

Brunner, D., Taeri-Baghbadrani, S., Sigle, W. and Rühle, M. (2001) Surprising results of a study on the plasticity in strontium titanate. *Journal of the American Ceramic Society*, **84**, 1161-1163.

Bulatov, V. V., Kaxiras E. (1997) Semidiscrete Variational Peierls Framework for Dislocation Core Properties. *Physical Review Letters*, **78**, 4221-4224

Burgers, J. M. (1939) Some considerations on the fields of stress connected with dislocations. *Proceedings of the Koninklijke Nederlandse Akademie van Wetenschappen,* **42**, 293.

Burton, W. K., Cabrera, N. and Frank, F. C. (1949) Role of dislocations in crystal growth. *Nature*, 163 398-399.

Cai, W., Bulatov, V. V., Chang, J., Li, J. and Yip, S. (2001) Anisotropic elastic interactions of a periodic dislocation array. *Physical Review Letters*, **86**, 5727-5730.

Cai, W., Bulatov, V. V., Chang, J., Li, J. and Yip, S. (2003) Periodic image effects in dislocation modelling. *Philosophical Magazine*, **83**, 539-567.

Carrez, P., Cordier, D., Mainprice, D. and Tommasi, A. (2006) Slip systems and plastic shear anisotropy in Mg_2SiO_4 ringwoodite: insights from numerical modelling. *European Journal of Mineralogy,* **18**, 149–160.

Carrez, P., Ferré, D. and Cordier, D. (2007a) Implications for plastic flow in the deep mantle from modelling dislocations in $MgSiO_3$ minerals. *Nature,* **446**, 68–70.

Carrez, P., Ferré, D. and Cordier, D. (2007b) Peierls-Nabarro model for dislocations in $MgSiO_3$ post-perovskite calculated at 120 GPa from first principles. *Philosophical Magazine,* **87**, 3229–3247.

Carrez, P., Walker, A.M., Metsue, A. and Cordier, D. (2008) Evidence from numerical modelling for 3D spreading of [001] screw dislocations in Mg_2SiO_4 forsterite. *Philosophical Magazine,* **88**, 2477–2485.

Carrez, P., Ferré, D. and Cordier, D. (2009a) Peierls-Nabarro modelling of dislocations in MgO from ambient pressure to 100 GPa. *Modelling and Simulation in Materials Science and Engineering,* **17**, art.num.035010. doi:10.1088/0965-0393/17/3/035010

Carrez, P., Ferré, D. and Cordier, D. (2009b) Thermal activation of dislocation glide in MgO based on an Elastic-Interaction model of kink-pair nucleation. *IOP Conference Series: Materials Science and Engineering,* **3**, art.num.012011. doi:10.1088/1757-899X/3/012011

Chen, J., Inoue, T., Weidner, D. J., Wu, Y. and Vaughan, M. T. (1998) Strength and water weakening of mantle minerals, olivine, wadsleyite and ringwoodite. *Geophysical Research Letters,* **25**, 575-578.

Christian J. W. and Vítek, V. (1970) Dislocations and stacking faults. *Reports on Progress in Physics*, **33**, 307-411.

Clouet, E. (2009) Elastic energy of a straight dislocation and contribution from core tractions. *Philosophical Magazine,* **89**, 1565–1584.

Clouet, E. Ventelon, L. and Willaime, F. (2009) Dislocation core energies and core fields from first principles. *Physical Review Letters,* **102**, art.num.055502.

Cordier, P. (2002) Dislocations and slip systems in mantle minerals. In S.-I. Karato and H.-R. Wenk, Eds. *Plastic deformation and deformation microstructure in Earth materials*. Reviews in Mineralogy, 51, 137-179. Mineralogical Society of America, Washington.

Cordier, P., Barbe, F., Durinck, J., Tommasi, A. and Walker A. M. (2005) Plastic deformation of minerals at high pressure: multiscale numerical modelling. In R. Miletich, Ed. *Mineral Behaviour at Extreme Conditions*. EMU Notes in Mineralogy 7, 389-415. Eötvös University Press, Budapest.

Couret A. and Calliard D. (1989) Prismatic slip in beryllium I. The controlling mechanism at the peak temperature. *Philosophical Magazine A*, **59**, 783-800.

Couvy, H., Frost, D. J., Heidelbach, F., Nyilas, K., Ungár, T., Mackwell, S. and Cordier, P. (2004) Shear deformation experiments of forsterite at 11 GPa - 1400°C in the multianvil apparatus. *European Journal of Mineralogy*, **16**, 877-889.

Davis, K. J., Dove, P. M. and De Yoreo, J. J. (2000) The role of Mg^{2+} as an impurity in calcite growth. *Science*, **290**, 1134-1137.

de Koning, M., Antonelli, A., Buzant, M. Z., Kaxiras, E. and Justo, J. F. (1998) Finite-temperature molecular dynamics study of unstable stacking fault free energies in silicon. *Physical Review B*, **58**, 12555-12558.

Denoual, C. (2004) Dynamic dislocation modeling by combining Peierls Nabarro and Galerkin methods. *Physical Review B*, **70**, art. num. 024106.

Denoual, C. (2007) Modeling dislocation by coupling Peierls-Nabarro and element-free Galerkin methods. *Computer Methods in Applied Mechanics and Engineering*, **196**, 1915-1923.

Dehlinger, U. (1929) Zur Theorie der Rekristallisation reiner Metalle. *Annalen der Physik*, **393**, 749-793.

Dorn, J. E. and Rajnak, S. (1964) Nucleation of kink pairs and the Peierls mechanism of plastic deformation. *Transactions of the Metallurgical Society of AIME*, **230**, 1052-1064

Dumrul, S., Bazzana, S., Warzywoda, J., Biederman, R. R. and Sacco, A. (2002) Imaging of crystal growth-induced fine surface features in zeolite A by atomic force microscopy. *Microporous and Mesoporous Materials*, **54**, 79–88.

Dupas, C., Doukhan, N., Doukhan, J.-C., Green, H. W., I. and Young, T. E. (1994) Analytical electron microscopy of a synthetic peridotite experimentally deformed in the β olivine stability field. *Journal of Geophysical Research,* **99**, 15821-15832.

Dupas-Bruzek, C., Sharp, T. G., Rubie, D. C. and Durham, W. B. (1998) Mechanisms of transformation and deformation in $Mg_{1.8}Fe_{0.2}SiO_4$ olivine and wadsleyite under non-hydrostaric stress. *Physics of the Earth and Planetary Interiors,* **108**, 33-48.

Durinck, J., Legris, A. and Cordier, P. (2005a) Influence of crystal chemistry on ideal plastic shear anisotropy in forsterite: First principle calculations. *American Mineralogist,* **90**, 1072–1077.

Durinck, J., Legris, A. and Cordier, P. (2005b) Pressure sensitivity of olivine slip systems: first-principle calculations of generalised stacking faults. *Physics and Chemistry of Minerals,* **32**, 646–654.

Durinck, J., Carrez, P. and Cordier, P. (2007) Application of the Peierls-Nabarro model to dislocations in forsterite. *European Journal of Mineralogy,* **19**, 631–639.

Ewels, C. P., Wilson, N. T., Heggie, M. I., Jones, R. and Briddon, P. R. (2001) Graphitization at diamond dislocation cores. *Journal of Physics: Condensed Matter*, **13**, 8965 - 8972.

Ferré, D., Carrez, P. and Cordier, P. (2007) First principles determination of dislocations properties of $MgSiO_3$ perovskite at 30 GPa based on the Peierls–Nabarro model. *Physics of the Earth and Planetary Interiors,* **163**, 283–291.

Ferré, D., Carrez, P. and Cordier, P. (2008) Modelling dislocation cores in $SiTiO_3$ using the Peierls-Nabaro model. *Physical Review B*, **77**, art.no.014106.

Ferré, D., Carrez, P. and Cordier, P. (2009a) Dislocation modeling in calcium silicate perovskite based on the Peierls-Nabarro model. *American Mineralogist,* **94**, 135–142.

Ferré, D., Carrez, P. and Cordier, P. (2009b) Peierls dislocation modelling in perovskite ($SaTiO_3$): comparison with tausonite ($SrTiO_3$) and $MgSiO_3$ perovskite. *Physics and Chemistry of Minerals,* **36**, 233–239.

Frank, F. C. (1951) Crystal dislocations - Elementary concepts and definitions. *Philosophical Magazine Series 7*, **42**, 809-819.

Frost, H. J. and Ashby, M. F. (1982) *Deformation-Mechanism Maps: The Plasticity and Creep of Metals and Ceramics*. Pergamon Press

Gaboriaud, R. J. (2009) Dislocation core and pipe diffusion in Y_2O_3. *Journal of Physics D: Applied Physics*, **42**, art. num. 135410.

Gale, J. D. and Rohl, A. L. (2003) The general utility lattice program (GULP). *Molecular Simulation*, **29**, 291-341.

Gehlen, P. C., Hirth, J. P., Hoagland, R. G., and Kanninen, M. F. (1972) A new representation of the strain field associated with the cube-edge dislocation of α-iron. *Journal of Applied Physics*, **43**, 3921-3933.

Gumbsch, P., Taeri-Baghbadrani, S., Brunner, D., Sigle, W. and Rühle, M. (2001) Plasticity and an inverse brittle-to-ductile transition in strontium titanate. *Physical Review Letters*, **87**, art. num. 085505

Hartford, J., von Sydow, B., Wahnström, G. and Lundqvist, B. I. (1998) Peierls barrier and stresses for edge dislocations in Pd and Al calculated from first principles. *Physical Review B*, **58**, 2487-2496.

Healy, D., Reddy, S. M., Timms, N. E., Gray, E. M. and Brovarone, A. V. (2009) Trench-parallel fast axes of seismic anisotropy due to fluid-filled cracks in subducting slabs. *Earth and Planetary Science Letters,* **283**, 75-86.

Heggie, M. I., Jenkins, S., Ewels, C. P., Jemmer, P., Jones, R. and Briddon, P. R. (2000) Theory of dislocations in diamond and silicon and their interactions with hydrogen. *Journal of Physics: Condensed Matter*, **12**, 10263 - 10270.

Heggie, M. I., Ewels, C. P., Martsinovich, N., Scarle, S., Jones, R., Goss, J. P., Hourahine, B. and Briddon, P. R. (2002) Glide dislocations in diamond: first-principles calculations of similarities with and differences from silicon and the effects of hydrogen. *Journal of Physics: Condensed Matter*, **14**, 12689-12696.

Hirose, K. (2006) Postperovskite phase transition and its geophysical implications. *Reviews of Geophysics*, **44**, RG3001.

Hirth, J. P. (1972) Anisotropic elastic solutions for line force arrays. *Scripta Metallurgica*, **6**, 535-540.

Hirth, J. P. and Lothe, J. (1984) *Theory of dislocations, second edition.* John Wiley and Sons.

Hoagland, R. G., Hirth, J. P., and Gehlen, P. C. (1976) Atomic simulation of the dislocation core structure and Peirels stress in alkali halide. *Philosophical Magazine*, **34**, 413-439.

Hunt, S. A., Weidner, D. J., Li, L., Wang, L., Walte, N. P., Brodholt, J. P. and Dobson, D. P. (2009) Weakening of calcium iridate during its transformation from perovskite to post-perovskite. *Nature Geoscience*, **2**, 794-797.

Hull, D. and Bacon, D. J., (1984) *Introduction to dislocations*, Pergamon Press, Oxford.

Hÿtch, M. J., Putaux, J.-L., and Pénisson, J. -M. (2003) Measurement of the displacement field of dislocations to 0.03 Å by electron microscopy. *Nature*, **423**, 270 - 273.

Hÿtch, M. J., Snoeck, E., and Kilaas, R. (1998) Quantitative measurement of displacement and strain fields from HRTEM micrographs. *Ultramicroscopy*, **74**, 131-146.

Ismail-Beigi, S., and Arias, T. A. (2000) Ab initio study of screw dislocations in Mo and Ta: a new picture of plasticity in bcc transition metals. *Physical Review Letters*, **84**, 1499-1502.

Iitaka, T., Hirose, K., Kawamura, K. and Murakami, M. (2004) The elasticity of the $MgSiO_3$ post-perovskite phase in the Earth's lowermost mantle. *Nature*, **430**, 442-445.

Jia, C. L., Thust, A. and Urban, K. (2005) Atomic-scale analysis of the oxygen configuration at a $SrTiO_3$ dislocation core. *Physical Review Letters,* **95**, art.num.225506.

Johnson, C. L., Hÿtch, M. J., Buseck, P. R. (2004) Displacement and strain fields around a[100] dislocation in olivine measured to sub-angstrom accuracy. *American Mineralogist*, **89**, 1374–1379.

Joós, B., Ren, Q. and Duesbery, M. S. (1994) Peierls-Nabarro model of dislocations in silicon with generalized stacking-fault restoring forces. *Physical Review B*, **50**, 5890-5898.

Jung, H. and Karato, S.-I. (2001) Water-induced fabric transition in olivine. *Science,* **293**, 1460-1463.

Jung, H., Katayama, I., Jiang, Z., Hiraga, T. and Karato, S.-I. (2006) Effect of water and stress on the Lattice preferred orientation in olivine. *Tectonophysics*, **421**, 1-22

Jung, H., Mo, W. and Green, H. W. (2009) Upper mantle seismic anisotropy resulting from pressure-induced slip transition in olivine. *Nature Geoscience*, **2**, 73-77.

Kaxiras, E. and Duesbery, M. S. (1993) Free energies of generalized stacking faults in Si and implications for the brittle-ductile transition. *Physical Review Letters*, **70**, 3752-3755.

Katayama, I. and Karato, S.-I. (2006) Effect of temperature on the B- to C-type olivine fabric transition and implications for flow pattern in subduction zones. *Physics of the Earth and Planetary Interiors*, **157**, 33-45.

Katayama, I. and Karato, S.-I. (2008) Low temperature high stress deformation of olivine under water saturated conditions. *Physics of the Earth and Planetary Interiors*, **168**, 125-133.

Katayama, I., Hirauchi, K., Michibayashi, K. and Ando, J. (2009) Trench-parallel anisotropy produced by serpentine deformation in the hydrated mantle wedge. *Nature,* **461**, 1114-1117.

Kaplan, T., Liu, F., Mostoller, M., Chisholm, M. F., and Milman, V. (2000) First-principles study of impurity segregation in edge dislocations in Si. *Physical Review B*, **61**, 1674-1676.

Kinsland, G. L. and Basset, W. A. (1977) Strength of MgO and NaCl polycrystals to confining pressures of 250 kbar at 25 °C. *Journal of Applied Physics,* **48**, 978-986.

Koizumi, H., Kirchner, H. O. K. and Suzuki, T. (1993) Kink pair nucleation and critical shear stress. *Acta Metallurgica et Materialia*, **41**, 3483-3493.

Kroupa, F. and Lejček, L. (1972) Splitting of dislocations in the Peierls-Nabarro model. *Czechoslovak Journal of Physics B*, **22**, 813-825.

Legros, M., Dehm, G., Arzt, E. and Balk, T. J. (2008) Observation of giant diffusivity along dislocation cores. *Science*, **319**, 1646-1649.

Lejček, L. (1972) Peierls-Nabarro model of planar dislocation cores in BCC crystals. *Czechoslovak Journal of Physics B*, **22**, 802-812.

Li., P., Karato, S.-I., and Wang, Z. (1996) High-temperature creep in fine-grained polycrystalline $CaTiO_3$, an analogue material of $(Mg,Fe)SiO_3$ perovskite. *Physics of the Earth and Planetary Interiors,* **95**, 19-36.

Li, J., Cai, W., Chang, J. and Yip, S. (2003) Atomistic measures of materials strength and deformation, In Catlow, C. R. A. and Kotomin (eds) *Computational Mineral Science*, NATO Science Series III, **187**, 359-387, IOS Press, Amsterdam.

Liu, F., Mostoller, M., Chisholm, M. F., and Kaplan, T. (1995) Electronic and elastic properties of edge dislocations in Si. *Physical Review B*, **51**, 17192-17195.

Love, A. E. H. (1920) *A Treatise on the Mathematical Theory of Elasticity*, 3rd edition, Cambridge University Press, Cambridge.

Lu, G. (2005) The Peierls-Nabarro Model of Dislocations: A venerable theory and its current development. In *Handbook of Materials Modeling. Volume 1: Methods and Models*. S. Yip, Ed. Springer. p. 1-19.

Martsinovich, N., Heggie, M. I. and Ewels, C. P. (2003) First-principles calculations on the structure of hydrogen aggregates in silicon and diamond *Journal of Physics: Condensed Matter*, **15**, S2815-S2824.

Matsunaga, T. and Saka, H. (2000) Transmission electron microscopy of dislocations in $SrTiO_3$. *Philosophical Magazine Letters*, **80**, 597-604.

Medvedeva, N. I., Mryasov, O. N., Gornostyrev, Y. N., Novikov, D. L. and Freeman, A. J. (1996) First-principles total-energy calculations for planar shear and cleavage decohesion processes in B2-ordered NiAl and FeAl. *Physical Review B*, **54**, 13506-13514.

Merkel, S., Kubo, A., Miyagi, L., Speziale, S., Duffy, T. S., Mao, H.-K. and Wenk, H.-R. (2006) Plastic Deformation of $MgGeO_3$ Post-Perovskite at Lower Mantle Pressures. *Science*, **311**, 644-646.

Merkel, S., McNamara, A. K., Kubo, A., Speziale, S., Miyagi, L., Meng, Y., Duffy, T. S. and Wenk, H.-R. (2007) Deformation of $(Mg,Fe)SiO_3$ Post-Perovskite and D" Anisotropy. *Science,* **316**, 1729-1732.

Metsue, A., Carrez, P., Mainprice, D. and Cordier, P. (2009) Numerical modelling of dislocations and deformation mechanisms in $CaIrO_3$ and $MgGeO_3$ post-perovskites - Comparison with $MgSiO_3$ post-perovskite. *Physics of the Earth and Planetary Interiors,* **174**, 165–173.

Metsue, A., Carrez, P., Denoual, C. and Cordier, P. (2010) Plastic deformation of wadsleyite: IV Dislocation core modelling based on the Peierls-Nabarro-Galerkin model. *Acta Materialia,* **58**, 1467-1478.

Miranda, C. R. and Scandolo, S. (2005) Computational materials science meets geophysics: dislocations and slip planes in MgO. *Computer Physics Communications*, **169**, 24-27.

Miyagi, L., Nishiyama, N., Wang, Y., Kubo, A., West, D. V., Cava, R. J., Duffy, T. S. and Wenk, H.-R. (2008) Deformation and texture development in $CaIrO_3$ post-perovskite phase up to 6 GPa and 1300 K. *Earth and Planetary Science Letters*, **268**, 515-525.

Miyagi, L., Merkel, S., Yagi, T., Sata, N., Ohishi, Y. and Wenk, H.-R. (2009) Diamond anvil cell deformation of $CaSiO_3$ perovskite up to 49 GPa. *Physics of the Earth and Planetary Interiors*, 174, 159-164.

Miyajima, M. and Walte, N. (2009) Burgers vector determination in deformed perovskite and post-perovskite of $CaIrO_3$ using thickness fringes in weak-beam dark-field images. *Ultramicroscopy*, **109**, 683-692.

Mookherjee, M., Stixrude, L. and Karki, B. (2008) Hydrous silicate melt at high pressure. *Nature*, **452**, 983-986.

Mossenfelder, J. L., Connolly, J. A. D., Rubie, D. C. and Liu, M. (2000) Strength of $(Mg,Fe)_2SiO_4$ wadsleyite determined by relaxation of transformation stress. *Physics of the Earth and Planetary Interiors,* **120**, 63-78.

Mryasov, O. N., Gornostyrev, Y. N. and Freeman, A. J. (1998) Generalized stacking-fault energetics and dislocation properties: compact versus spread unit-dislocation structures in TiAl and CuAu. *Physical Review B*, **58**, 11927-11932.

Murakami, M., Hirose, K., Kawamura, K., Sata, N. and Ohishi, Y. (2004) Post-perovskite phase transition in $MgSiO_3$. *Science*, **304**, 855-858.

Nabarro, F. R. N. (1947) Dislocations in a simple cubic lattice. *Proceedings of the Physical Society of London*, **59**, 256–272.

Narayan, J., and Washburn, J. (1972) Self-climb of dislocation loops in magnesium oxide. *Philosophical Magazine*, **26**, 1179-1190.

Nishigaki, J., Kuroda, K. and Saka, H. (1991) Electron microscopy of dislocation structures in $SrTiO_3$ deformed at high temperatures. *Physica Status Solidi (a),* **128**, 319-336.

Nishihara, Y., Tinker, D., Kawazoe, T., Xu, Y., Jing, Z., Matsukage, K. N. and Karato, S.-I. (2008) Plastic deformation of wadsleyite and olivine at high-pressure and high-temperature using a rotational Drickamer apparatus (RDA). *Physics of the Earth and Planetary Interiors,* **170**, 156-169.

Niwa, K., Yagi, T., Ohgushi, K., Merkel, S., Miyajima, N. and Kikegawa, T. (2007) Lattice preferred orientation in $CaIrO_3$ perovskite and post-perovskite formed by plastic deformation under pressure. *Physics and Chemistry of Minerals*, **34**, 679-686,

Nocedal, J. (1980) Updating quasi-Newton matrices with limited storage. *Mathematics of Computation*, **25**, 773-782.

Oganov, A. R. and Ono, S. (2004) Theoretical and experimental evidence for a post-perovskite phase of $MgSiO_3$ in Earth's D" layer. *Nature,* **430**, 445-448.

Oganov, A. R., Martoňák, R., Laio, A., Raiteri, P. and Parrinello, M. (2004) Anisotropy of Earth's D" layer and stacking faults in the $MgSiO_3$ post-perovskite phase. *Nature,* **438**, 1142-1144.

Orowan, E. (1934) Zur Kristallplastizität I-III. *Zeitschrift für Physik A Hadrons and Nuclei*, **89**, 605-659.

Peierls, R. E. (1940) On the size of a dislocation. *Proceedings of the Physical Society of London*, **52**, 34–37.

Pizzagalli, L., Godet, J. and Brochard, S. (2009) Glissile dislocations with transient cores in silicon. *Physical Review Letters,* **103**, art. num. 065505.

Poirier, J.-P. (1985) *Creep of crystals. High-temperature deformation processes in metals, ceramics and minerals*, Cambridge University Press, Cambridge.

Polanyi, M. (1934) Über eine Art Gitterstörung, die einen Kristall plastisch machen könnte. *Zeitschrift für Physik A Hadrons and Nucle*i, **89**, 660-664

Prandtl, L. (1928) Hypothetical model for the kinetic theory of solid bodies. *Zeitschrift für Angewandte Mathematik und Mechanik*, **8**, 85.

Puls, M. P. (1980) Vacancy-dislocation interaction energies in MgO. *Philosophical Magazine A*, **41**, 353-368.

Puls, M. P. (1983) Vacancy-dislocation interactions energies in MgO A re-analysis. *Philosophical Magazine A*, **47**, 497-513.

Puls, M. P., and Norgett, M. J. (1976) Atomic calculation of the core structure and Peierls energy of an (a/2)[110] edge dislocation in MgO. *Journal of Applied Physics*, **47**, 466-477.

Puls, M. P., Woo, C. H., and Norgett, M. J. (1977) Shell-model calculations of interaction energies between point defects and dislocations in ionic crystals. *Philosophical Magazine*, **36**, 1457-1472.

Rabier, J., and Puls, M. P. (1989) On the core structures of edge dislocations in NaCl and MgO. Consequences for the core configurations of dislocation dipoles. *Philosophical Magazine A*, **59**, 821-842.

Rabier, J., Soullard, J., and Puls, M. P. (1990) Atomic calculations of point-defect interactions with an edge dislocation in NiO. *Philosophical Magazine A*, **61**, 99-108.

Rao, S. I., Hernandez, C., Simmons, J. P., Parthasarathy, T. A. and Woodward, C. (1998) Green's function boundary conditions in two-dimensional and three-dimensional atomistic simulations of dislocations. *Philosophical Magazine A*, **77**, 231-256.

Rao, S. I., Parthasarathy, T. A. and Woodward, C. (1999) Atomistic simulation of cross-slip processes in model fcc structures. *Philosophical Magazine A*, **79**, 1167-1192.

Raterron, P., Chen, J., Li., L., Weidner, D. and Cordier, P. (2007) Pressure-induced slip-system transition in forsterite: Single-crystal rheological properties at mantle pressure and temperature. *American Mineralogist*, **92**, 1436-1445.

Raterron, P., Amiguet, E., Chen, J., Li, L. and Cordier, P. (2009) Experimental deformation of olivine single crystals at mantle pressures and temperatures. *Physics of the Earth and Planetary Interiors*, **172**, 74–83.

Reddy, S. M., Timms, N. E., Trimby, P., Kinny, P. D., Buchan, C. and Blake, K. (2006) Crystal-plastic deformation of zircon: A defect in the assumption of chemical robustness. *Geology*, **34**, 257-260.

Russo, R. M. and Silver, P. G. (1994) Trench-parallel flow beneath the Nazca plate from seismic anisotropy. *Science*, **263**, 1105-1111.

Sakaguchi, I. Yurimota, H. and Sueno, S. (1992) Self-diffusion along dislocations in single-crystal MgO. *Solid State Communications*, **84**, 889-893.

Saunders, V. R., Freyria-Fava, C., Dovesi, R., and Roetti, C. (1994) On the electrostatic potential in linear periodic polymers. *Computer Physics Communications*, **84**, 156 - 172.

Seeger, A. (1981) The kink picture of dislocation mobility and dislocation-point-defect interactions. *Journal de Physique*, **42**, 201-228.

Sharp, T. G., Bussod, G. Y. A. and Katsura, T. (1994) Microstructures in beta-$Mg_{1.8}Fe_{0.2}SiO_4$ experimentally deformed at transition-zone conditions. *Physics of the Earth and Planetary Interiors,* **86**, 69-83.

Sinclair, J. E. (1971) Improved atomistic model of a bcc dislocation core. *Journal of Applied Physics*, **42**, 5321-5329.

Sinclair, J. E., Gehlen, P. C., Hoagland, R. G., and Hirth, J. P. (1978) Flexible boundary conditions and nonlinear geometric effects in atomic dislocation modeling. *Journal of Applied Physics*, **49**, 3890-3897.

Schoeck, G. (1996) Dislocation emission from crack tips as a variational problem of the crack energy. *Journal of the Mechanics and Physics of Solids*, **44**, 413-437.

Schoeck, G. (1997) The core structure of «001» dislocations in bcc metals. *Philosophical Magazine Letters,* **76**, 15-24.

Schoeck, G. (1999a) Peierls energy of dislocations: A critical assessment. *Physical Review Letters,* **82**, 2310-2313.

Schoeck, G. (1999b) The Peierls energy revisited. *Philosophical Magazine A*, **79**, 2629-2636.

Schoeck, G. (2005) The Peierls model: Progress and limitations. *Materials Science and Engineering A*, **400-401**, 7-17.

Schoeck, G. and Krystian, M. (2005) The Peierls energy and kink energy in fcc metals. *Philosophical Magazine*, **85**, 949-966

Steeds, J. W., (1973) *Introduction to anisotropic theory of dislocations*. Oxford University Press, Oxford.

Steeds, J. W. and Willis, J. R. (1979) Dislocations in anisotropic media. In F. N. R. Nabarro, Ed. *Dislocations in Solids, The Elastic Theory*, **1**, 143-165. North-Holland Publishing Company, Amsterdam.

Stroth, A. N. (1958) Dislocations and cracks in anisotropic elasticity. *Philosophical Magazine*, **3**, 625-646.

Suarez-Martinez, I., Savini, G., Haffenden, G., Campanera, J.-M. and Heggie, M. I. (2007) Dislocations of Burgers vector *c*/2 in graphite. *Physica Status Solidi (c)*, **4**, 2958-2962.

Sun, Y. and Kaxiras, E. (1997) Slip energy barrier in aluminium and implications for ductile-brittle behaviour. *Philosophical Magazine A*, **75**, 1117-1127.

Sunagawa, I. and Tsukamoto, K. (1972) Growth spirals on NaCl and KCl crystals grown from solution phase. *Journal of Crystal Growth*, **15**, 73-78.

Taylor, G. I. (1934) The mechanism of plastic deformation of crystals. *Part I - Theoretical. Proceedings of the Royal Society of London*, **145**, 362-387.

Thurel, E. and Cordier, P. (2003) Plastic deformation of wadsleyite: I. high pressure deformation in compression. *Physics and Chemistry of Minerals*, **30**, 256–266.

Thurel, E., Cordier, P., Frost, D. and Karato, S-I. (2003a) Plastic deformation of wadsleyite: II. high pressure deformation in shear. *Physics and Chemistry of Minerals*, **30**, 267–270.

Thurel, E., Douin, J. and Cordier, P. (2003b) Plastic deformation of wadsleyite: III. interpretation of dislocations and slip systems. *Physics and Chemistry of Minerals*, **30**, 271–279.

Tsuchiya, T., Tsuchiya, J., Umemoto, K. and Wentzcovitch, R. M. (2004) Phase Transition in $MgSiO_3$-perovskite in the Earth's Lower Mantle. *Earth and Planetary Science Letters*, **224**, 241-248.

Verma, A. K. and Karki, B. B. (2009) Ab initio investigation of native and protonic point defects in Mg_2SiO_4 polymorphs under high pressure. *Earth and Planetary Science Letters*, **285**, 140-149.

Vítek, V. (1966) Thermally activated motion of screw dislocations in B.C.C. metals. *Physica Status Solidi (b)*, **18**, 687-701.

Vítek, V. (1968) Intrinsic stacking faults in body-centred cubic crystals. *Philosophical Magazine*, **18**, 773-786.

Vítek, V., Perrin, R. C. and Bowen, D. K. (1970) The core structure of (111) screw dislocations in b.c.c. crystals. *Philosophical Magazine*, **21**, 1049-1073.

Volterra, V. (1907) Sur l'équilibre des corps élastiques multiplement connexes. *Annales Scientifiques de l'Ecole Normale Supérieure*, **24**, 401-517.

Walker, A. M. (2010) Simulation of screw dislocations in wadsleyite. *Physics and Chemistry of Minerals*, In Press, available online at doi:10.1007/s00269-009-0334-y

Walker, A. M., Wright, K. and Slater, B. (2003) A computational study of oxygen diffusion in olivine. *Physics and Chemistry of Minerals*, **30**, 536-545.

Walker, A. M., Slater, B., Gale, J. D. and Wright, K. (2004), Predicting the structure of screw dislocations in nanoporous materials. *Nature Materials*, **3**, 715-720.

Walker, A. M., Gale, J. D., Slater, B. and Wright, K. (2005a) Atomic scale modelling of the cores of dislocations in complex materials part 1: methodology. *Physical Chemistry Chemical Physics*, 7, 3227-3234.

Walker, A. M., Gale, J. D., Slater, B. and Wright, K. (2005b) Atomic scale modelling of the cores of dislocations in complex materials part 2: applications. *Physical Chemistry Chemical Physics*, **7**, 3235-3242.

Walker, A. M., Hermann, J., Berry, A. J. and O'Neill, H. St. C. (2007) Three water sites in upper mantle olivine and the role of titanium in the water weakening mechanism. *Journal of Geophysical Research*, **112**, art. no. B05211

Walker, A. M., Zhang, F., Wright K. and Gale, J. D. (2009) Magnesium Vacancy Segregation and Fast Pipe Diffusion for the 1/2<110>{110} Edge Dislocation in MgO, *EOS Transactions of the AGU*, **90**, fall meeting supplement, abstract MR23B-06.

Walte, N. P., Heidelbach, F., Miyajima, N., Frost, D. J, Rubie, D. C. and Dobson, D. P. (2009) Transformation textures in post-perovskite: Understanding mantle flow in the D″ layer of the Earth. *Geophysical Research Letters*, **36**, L04302.

Wang, Y., Durham, W. B., Getting, I. and Weidner, D. J. (2003) The deformation-DIA: a new apparatus for high-temperature triaxial deformation to pressures up to 15 GPa. *Review of Scientific Instruments,* **74**, 3002–11.

Watson, G. W., Kelsey, E. T., de Leeuw, N. H., Harris, D. J. and Parker, S. C. (1996) Atomistic simulation of dislocations, surfaces and interfaces in MgO. *Journal of the Chemical Society, Faraday Transactions*, **92**, 433–438.

Watson, G. W., Kelsey, E. T. and Parker S. C. (1999) Atomistic simulation of screw dislocations in rock salt structured materials. *Philosophical Magazine A*, **79**, 527–536.

Watson, G. W., Oliver, P. M., and Parker, S. C. (2001) Atomistic simulation of crystal growth at the a<100> screw dislocation terminating at the {100} surface of MgO. *Surface Science Letters*, **474**, L185 - L190.

Wolf, D., Keblinski, P., Phillpot, S. R. and Eggebrecht, J. (1999) Exact method for the simulation of Coulombic systems by spherically truncated, pairwise r^{-1} summation. *Journal of Chemical Physics*,**110**, 8254–8282.

Woo, C.H., and Puls, M.P. (1976) An improved method of calculating the lattice friction stress using an atomistic model. *Journal of Physics C: Solid State Physics*, **9**, L27-L31.

Woo, C.H., and Puls, M.P. (1977a) Atomistic breathing shell model calculations of dislocation core configurations in ionic crystals. *Philosophical Magazine*, **35**, 727-756.

Woo, C.H., and Puls, M.P. (1977b) The Peierls mechanism in MgO. *Philosophical Magazine*, **35**, 1641-1652.

Woodward, C. (2005) First-principles simulations of dislocation cores. *Materials Science and Engineering A*, **400-401**, 59-67.

Woodward, C. and Rao, S. I. (2002) Flexible *ab initio* boundary conditions: Simulating isolated dislocations in bcc Mo and Ta. *Physical Research Letters*, **88**, art num 216402.

Woodward, C., Trinkle, D. R., Hector, L., G., Jr. and Olmsted, D. L. (2008) Prediction of dislocation cores in aluminium from density functional theory. *Physical Review Letters*, **100**, art num 045507.

Wookey, J., Stackhouse, S., Kendall, J. M., Brodholt, J. P. and Price, G. D. (2005) Efficacy of the post-perovskite phase as an explanation for lowermost-mantle seismic properties. *Nature*, **438**, 1004-1007.

Wright, K., Price, G. D. and Poirier, J. P. (1992) High Temperature Creep of the Perovskites $CaTiO_3$ and $NaNbO_3$. *Physics of the Earth and Planetary Interiors*, **74**, 9-22.

Xu, G. and Argon, A. S. (2001) Energetics of homogeneous nucleation of dislocation loops under a simple shear stress in perfect crystals. *Materials Science and Engineering A*, **319-321**, 144-147.

Yamazaki, D. and Karato, S.-I. (2001) High-pressure rotational deformation apparatus to 15 GPa. *Review of Scientific Instruments*, **72**, 4207–11.

Zhang, Z., Sigle, W. and Rühle, M. (2002a) Atomic and electronic characterization of the a[100] dislocation core in $SrTiO_3$. *Physical Review B*, **66**, art no. 094108.

Zhang, Z., Sigle, W., Kurtz, W. and Rühle, M. (2002b) Electronic and atomic structure of a dissociated dislocation in $SrTiO_3$. *Physical Review B*, **66**, art no. 214112.

Tables

Symbol	Meaning
x ; y ; z	Cartesian coordinate system for crystal containing dislocation. z is aligned along the dislocation line.
u_x ; u_y ; u_z	Components of the displacement field around a dislocation.
b	Burgers vector
r	Radius of crystal containing a dislocation
r_0	Radius of dislocation core / hole
v	Poisson's ratio
μ	Shear modulus
K	Anisotropic energy factor
γ	Generalised stacking fault energy
a	Crystal periodicity in direction of Burgers vector (in Peierls-Nabarro model)
$S(x)$	Mismatch function in Peierls-Nabarro model
$\rho(x)$	Local dislocation density in Peierls-Nabarro model
$W(u)$	Energy cost of moving dislocation in Peierls-Nabarro model

Table 1: Selected list of symbols used in the text. The convention used thorough out this work is for the dislocation line to lies along the *z* Cartesian axis. Screw dislocations then have a Burgers vector parallel to *z* and edge and mixed dislocations have a Burgers vector in the *xz* plane (*y* is perpendicular to the glide plane).

Model	Peierls energy ($\times 10^{-3}$ eV/Å)	Peierls stress (MPa)
Cluster based rigid ion model	0.78	46
Cluster based shell model	0.81	47
Cluster based breathing shell model 1	1.40	76
Cluster based breathing shell model 2	1.24	69
Peierls-Nabarro model with DFT	0.13	20

Table 2: Peierls energy barrier height and Peierls stress for the $1/2\langle 1\bar{1}0 \rangle \{110\}$ edge dislocation MgO calculated using cluster based (Woo and Puls, 1977b) and PN models (Carrez *et al.,* 2009a). The PN model is based on DFT calculations of the GSF energy while the cluster based models utilise different interatomic potential models.

Cubic	Orthorhombic	$SrTiO_3$ (GPa)	$CaSiO_3$ (GPa)	$CaTiO_3$ (GPa)	$MgSiO_3$ (GPa)

$\langle 100 \rangle_c \{010\}_c$	$[100]_c(010)_c$	$[110]_o(\bar{1}10)_o$	0.7	1.9	6	33.6
	$[010]_c(001)_c$	$[\bar{1}10]_o(001)_o$			2	34.3
	$[001]_c(010)_c$	$[001]_o(\bar{1}10)_o$			8.7	33,9
$\langle 100 \rangle_c \{011\}_c$	$[001]_c(110)_c$	$[001]_o(010)_o$	9.9	6.7	16.6	44.1
	$[001]_c(1\bar{1}0)_c$	$[001]_o(100)_o$			11	23.6
$\langle 110 \rangle_c \{001\}_c$	$[110]_c(001)_c$	$[010]_o(001)_o$	0.9	1.4	8	22.6
	$[1\bar{1}0]_c(001)_c$	$[100]_o(001)_o$			9	39.2
$\langle 110 \rangle_c \{1\bar{1}0\}_c$	$[1\bar{1}0]_c(110)_c$	$[100]_o(010)_o$	0.006	0.02	5.5	15.5
	$[110]_c(1\bar{1}0)_c$	$[010]_o(100)_o$			5.8	8.3

Table 3: Peierls stresses for screw dislocation in perovskite structured minerals.

Figures

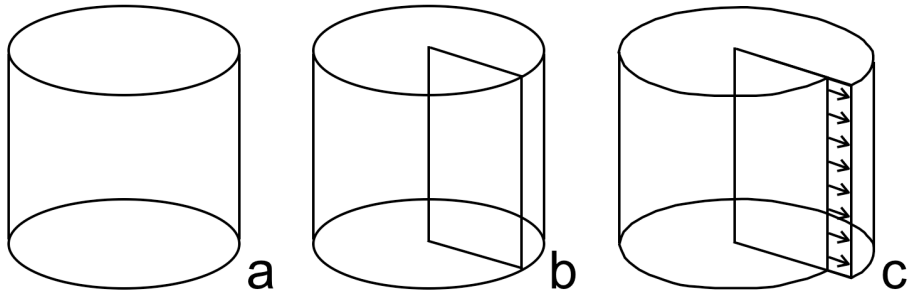

Figure 1

Figure 1: Conceptual model of the introduction of an edge dislocation into an elastic body. An undeformed elastic body (a) is modified by the introduction of a cut from the edge of the body to the centre (b) and the two sides of the cut are displaced (c) before being cemented together and the body allowed to reach elastic equilibrium. For an isotropic elastic body the resulting displacement between any point in the undeformed and deformed elastic body is given by Equation 2. Note that the necessary hole along the termination of the cut in the centre of the body is not shown.

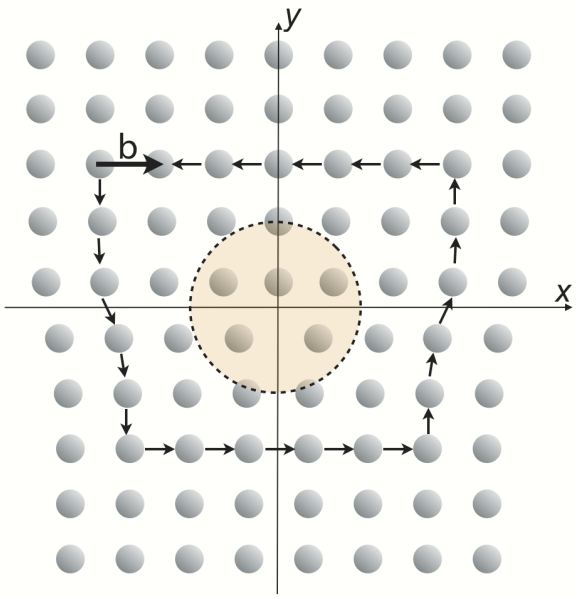

Figure 2

Figure 2: Geometry of an edge dislocation in a square lattice. The magnitude of the dislocation is described by the Burgers vector, the vector which closes a loop threading the dislocation core that would be closed in a perfect crystal. The locus of points around which the loop is not closed defined the dislocation line (extending perpendicular to the page in this example). The relationship between the Burgers vector and the vector describing the dislocation line determined the character of the dislocation (in this case they are perpendicular and the dislocation has an edge character, if they are parallel the dislocation has a screw character, mixed dislocations are also possible). In the shaded central region of the figure there is no direct mapping between the structure of the dislocation and that of a perfect reference crystal, the shaded region described as ‘bad’ crystal and contains the dislocation core.

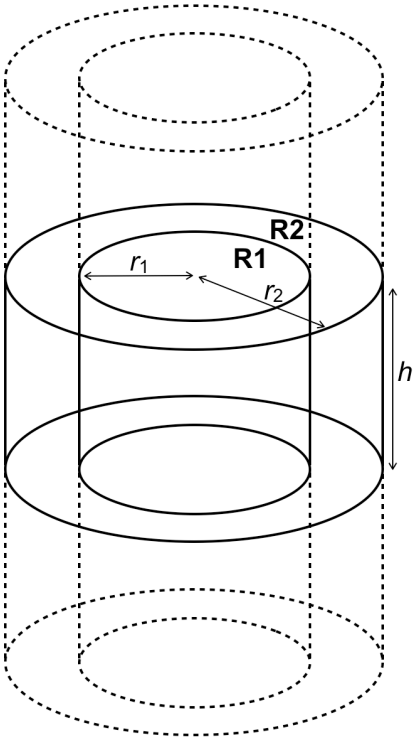

Figure 3

Figure 3: Basic simulation geometry used for 1D cluster type simulation of dislocations. A central simulation cell and two adjacent periodic images are shown in solid and broken lines, respectively. During the geometry optimisation, atoms close to the dislocation core (in the volume marked R1) are free to move to minimise the energy of the system while an outer sheath of atoms (in the volume marked R2) are either fixed at locations predicted from linear elasticity for a hollow core Volterra dislocation (fixed boundary conditions), or updated according to an iterative update that responds to elastically to forces generated by the core (flexible boundary conditions). Two radii, r_1 and r_2, and a periodicity along the dislocation line, h, define the size of the simulation cell.

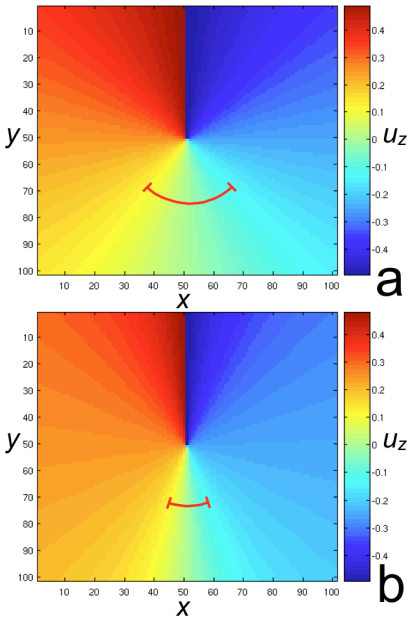

Figure 4

Figure 4: Linear elastic displacement field around screw dislocations in isotropic and simple anisotropic crystals. (a) For an isotropic crystal, or when the dislocation line lies along a four-fold rotation axis, the displacement increases smoothly with the angle around the dislocation line. (b) For an orthorhombic anisotropic crystal the pitch of the screw dislocation varies with angle around the dislocation line. The difference is highlighted by the red arcs which represent 1/4 of the total displacement around the dislocation and show the effect of the soft elastic constant in the orthorhombic case.

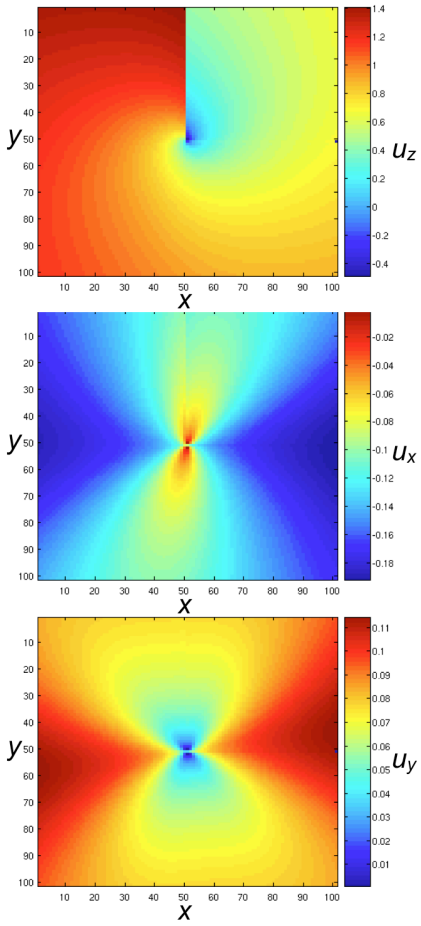

Figure 5

Figure 5: Linear elastic displacement field around a screw dislocation in a fully anisotropic (triclinic) crystal. Unlike the case shown in Figure 4, the displacement field has components in all three directions.

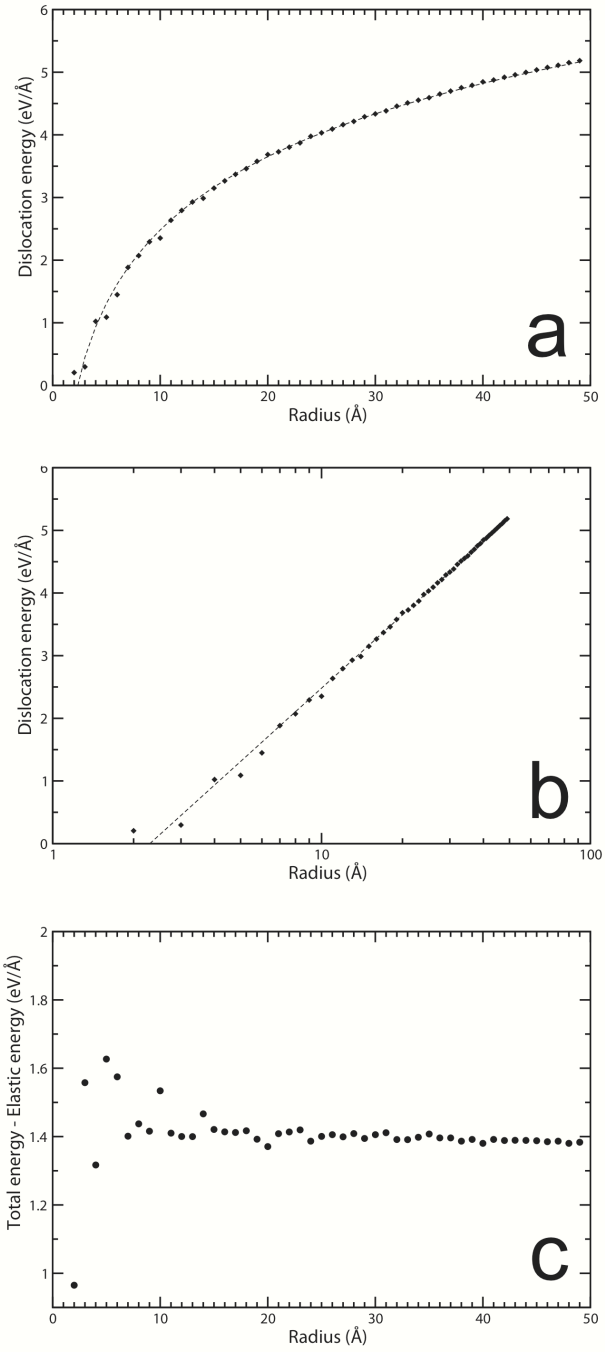

Figure 6: Energy extracted from an atomistic simulation of a dislocation, the data is from a model of the [100] screw dislocation in wadsleyite reported by Walker (2010). (a) Shows the total energy stored in a cylinder inside the simulation cell as a function of cylinder radius. (b) Shows this data plotted on a logarithmic axis which highlights the functional dependence of the elastic energy on radius. (c) Shows the core contribution to the total energy as a function of cylinder radius, found by subtracting the elastic energy from the data shown in (a). For large radii this converges on the core energy.

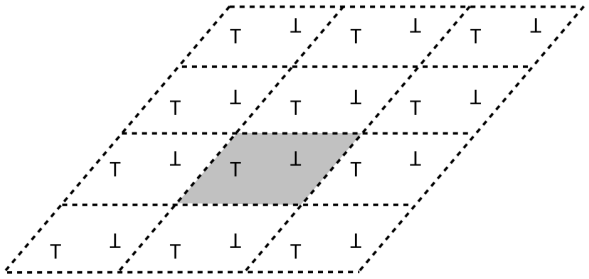

Figure 7

Figure 7: Arrangement of dislocations for to allow fully periodic dipole modelling of dislocations.

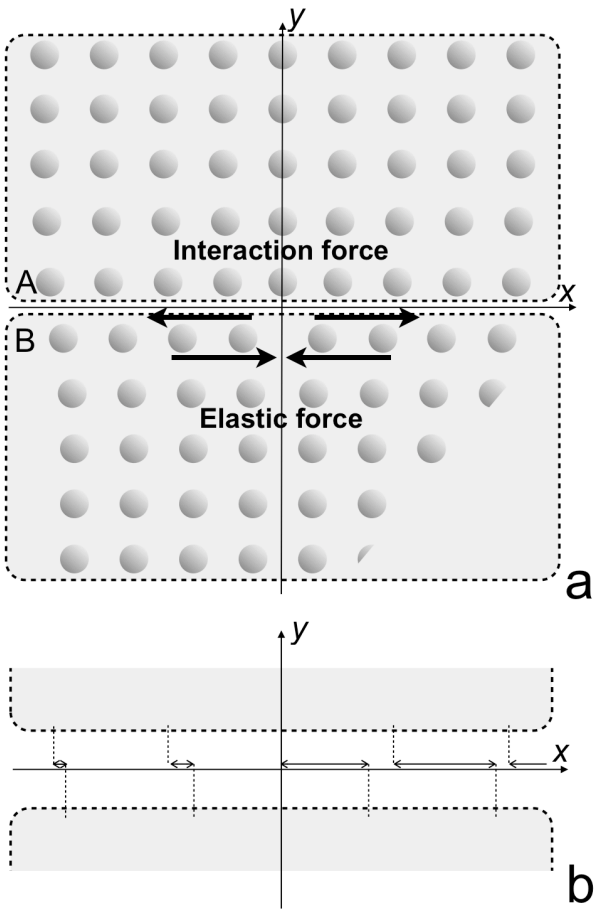

Figure 8

Figure 8: Illustration of the Peierls-Nabarro model. The crystal is separated into two bodies described using linear elasticity as shown in (a). In each half crystal experiences an internal elastic force and an interaction force from the other half crystal. The forces acting on the plane of atoms labelled “B” (on the top of the lower half-crystal) are represented by the pairs of arrows in (a). At equilibrium these forces balance leading to a mismatch across the glide plane, shown as the smaller arrows in (b).

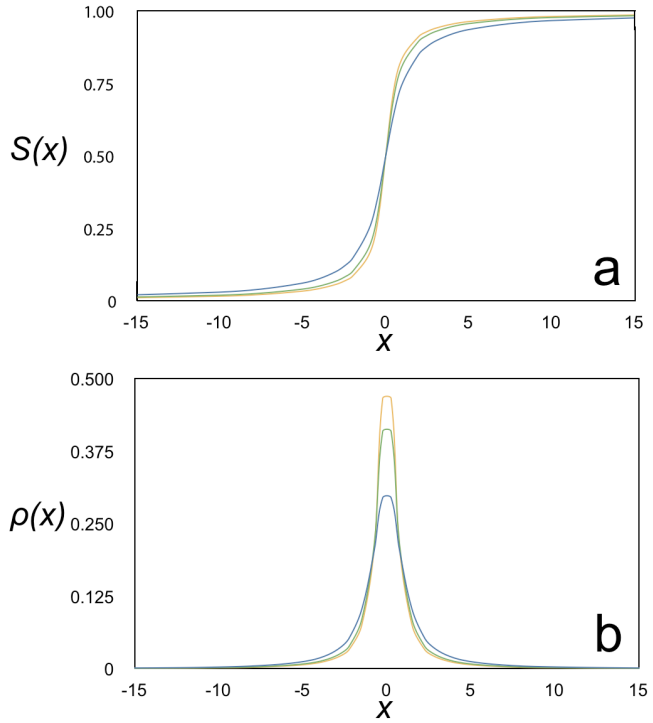

Figure 9

Figure 9: Solutions to the Peierls-Nabarro model for an elastically isotropic crystal with a sinusoidal restoring force (Equations 6 and 7) with three different values of Poisson's ratio (blue: 0.5, green 0.25, orange: 0.1). (a) The mismatch function. (b) The local dislocation density distribution.

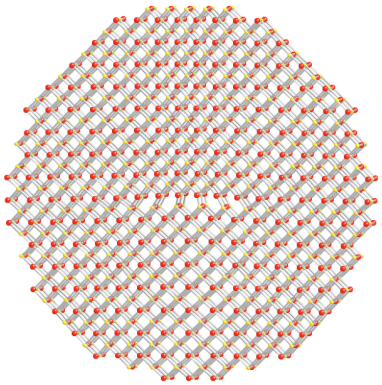

Figure 10

Figure 10: Structure of the 1/2 <110>{1-10} edge dislocation in MgO extracted from the Peierls-Nabarro modelling of (Carrez *et al.*, 2009a) using Equation 16.

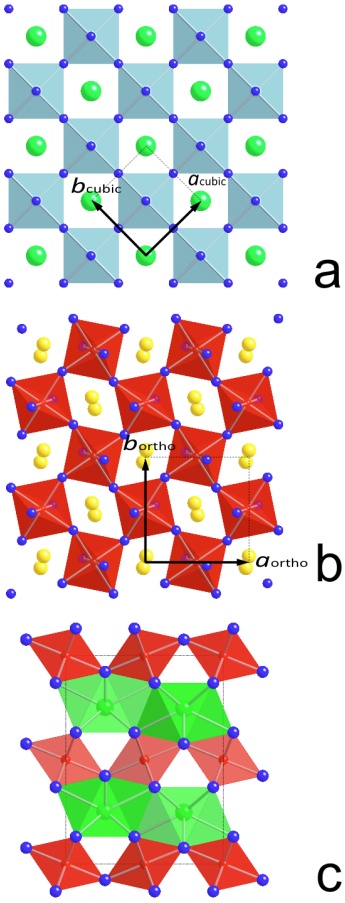

Figure 11

Figure 11: Structures of tausonite ($SrTiO_3$), a cubic perovskite (a), orthorhombic $MgSiO_3$ perovskite (b) and $MgSiO_3$ post-perovskite (c). In (a) and (b) the 'A' cation sites are shown as isolated spheres while the octahedral 'B' sites are shown as filled shapes.

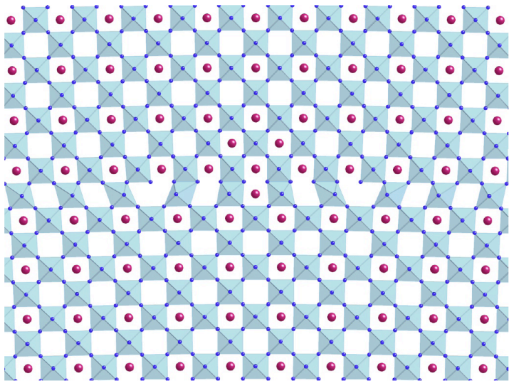

Figure 12

Figure 12: Core structure of <110>{$1\bar{1}0$} dislocation in $SrTiO_3$ from Peierls-Nabarro modelling showing how the pair of partial dislocations joined by a stacking fault leads to edge sharing octahedra.

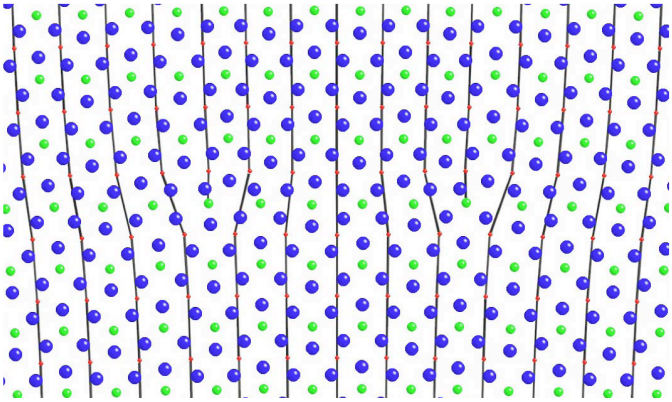

Figure 13

Figure 13: Core structure of [001](010) edge dislocation in $MgSiO_3$ post perovskite from Peierls-Nabarro modelling. The two partial dislocations lower the elastic energy of the dislocation (which has a large Burgers vector). This figure is reproduced from the original publication in *Nature* (Carrez *et al.*, 2009a).

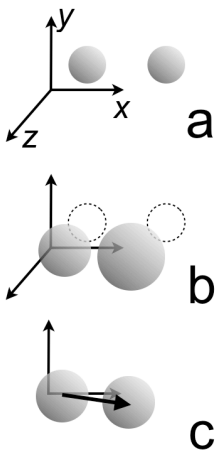

Figure 14

Figure 14: Outline of the construction of the Vítek representation for a screw dislocation. Two adjacent atoms in the un-dislocated crystal are at different positions relative to the incipient dislocation line (a). In introducing the dislocation the elastic displacement and atomistic reconstruction lead to different total displacements for the two atoms as they move from a location in the un-dislocated crystal to a new location in the dislocated crystal (b). The difference in the *z* component of the total displacements is calculated and represented as a vector plotted between the two atoms (c). Note that the axes are rotated in (c) compared to (a) and (b).

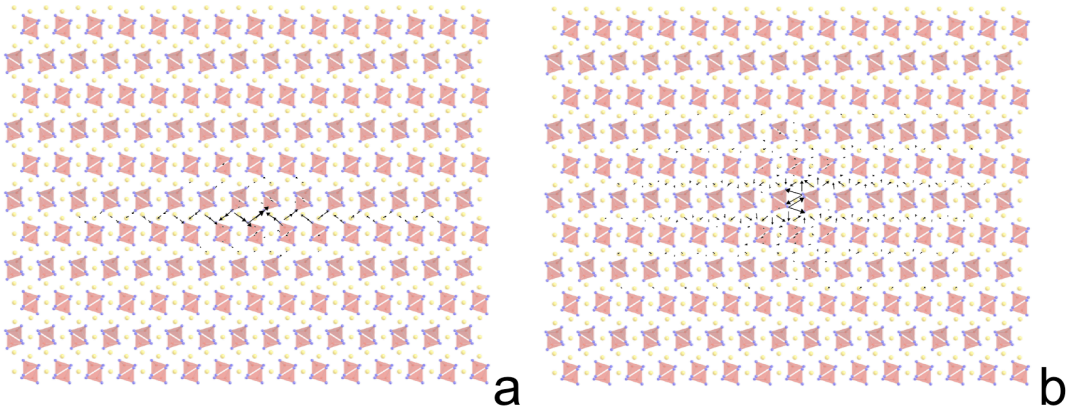

Figure 15

Figure 15: Vítek representation of the [001] screw dislocation in forsterite calculated using the Peierls-Nabarro (a) and cluster (b) models. The differential displacement is concentrated on a chosen (010) plane in (a) while it is distributed over several planes in (b).

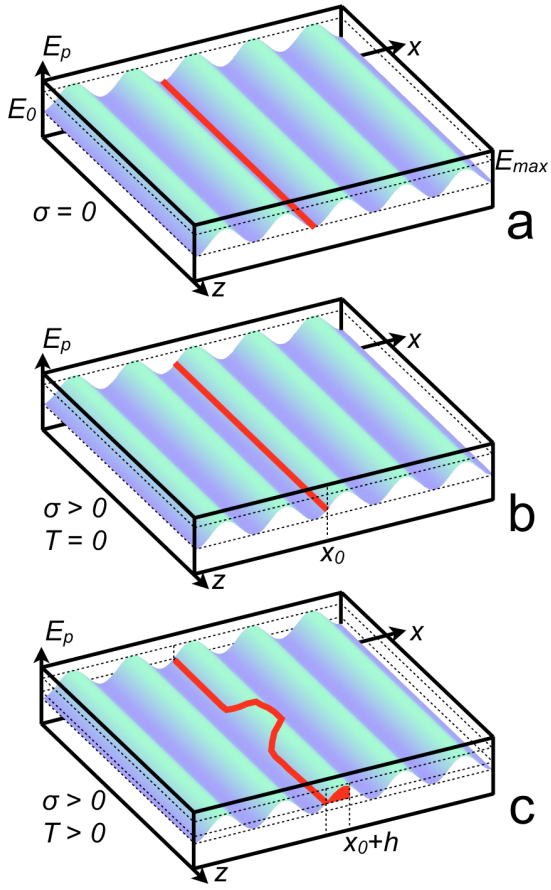

Figure 16

Figure 16: Kink nucleation and thermally activated glide. In (a) the crystal periodicity leads to periodic energy barriers (the Peierls potential, E_p) resisting movement of the dislocation in the glide plane. With no applied stress the dislocation will lay along the low energy 'valley' in the Peierls potential. At zero K the application of stress (b) will move the dislocation out of the bottom of the valley. Plastic deformation is only possible if the stress is more than the Peierls stress, otherwise the dislocation will only be slightly displaced. At finite temperature (c), thermal fluctuations can help a portion of the dislocation line to overcome the Peierls potential barrier at stresses lower than the Peierls stress leading to a flow law that depends on both stress and temperature.